A rapid and objective characterization of channel morphology in a small, forested channel using a remotely piloted aircraft.

by

Carina Helm

B.Sc., The University of British Columbia, 2017

A THESIS SUBMITTED IN PARTIAL FULFILMENT OF
THE REQUIREMENTS FOR THE DEGREE OF

Master of Science

in

THE FACULTY OF GRADUATE AND POSTDOCTORAL STUDIES

(Geography)

THE UNIVERSITY OF BRITISH COLUMBIA

(Vancouver)

August 2019

The following individuals certify that they have read, and recommend to the Faculty of Graduate and Postdoctoral Studies for acceptance, a thesis/dissertation entitled:

A rapid and objective characterization of channel morphology in a small, forested channel using a remotely piloted aircraft.

submitted by: Carina J. Z. Helm in partial fulfillment of the requirements
for the degree of Master of Science
in Geography

Examining Committee:

Marwan Hassan, Geography
Supervisor

John Richardson, Forest and Conservation Sciences
Supervisory Committee Member

Jennifer Williams, Geography
Additional Examiner

Abstract

The use of remotely piloted aircrafts (RPAs) in fluvial geomorphology has improved the ability to characterize streams at greater resolutions and spatial extents than was previously attainable using traditional survey techniques. However, their use has been generally limited to streams under ideal conditions that differ from the small, forested mountain channels common in the Pacific Northwest. These channels have remained difficult to characterize using modern techniques due to their dense canopies and rough terrain. A rapid and objective method of characterizing channel morphology across the river basin using a RPA is presented in this dissertation to help overcome this challenge. First, the accuracy of RPAs for extracting bed elevations, bathymetry and grain size along 3 km of Carnation Creek, a small, forested stream on Vancouver Island, was investigated through a sub-canopy survey. Relevant cross-sectional channel variables were then extracted to objectively characterize channel morphologies across the river basin using a principal component analysis-clustering (PCA-clustering) technique. Then the Shannon's diversity index was used to characterize the local diversity across the channel, and investigate the scale needed to study the system, to ensure its heterogeneity was characterized. The results demonstrate that RPAs provide a rapid alternative to characterizing these systems, through the construction of a 2–cm resolution digital elevation model spanning 3 km of channel, with a root-mean-square-error of 0.093 m for exposed bed check points and 0.1 m for submerged bed check points. The PCA-clustering analysis provided an objective means of classifying channel morphology with a correct classification rate of 85%. Altogether, the results provide a precedent for using a RPA to characterize the morphology and diversity of small, forested channels at a scale of ecological relevance to the life histories of Pacific salmonids.

Lay Summary

The use of remotely piloted aircrafts (also known as drones) in surveying stream systems has become well established in the last decade. However, to date these applications have been limited to streams with wide channels and minimal overhanging forest vegetation. The objective of this dissertation is to demonstrate the utility of remotely piloted aircrafts for sub-canopy surveying of a small, forested mountain channel at the basin-scale. The results provide a rapid and objective method for characterizing patterns in channel morphology and habitat diversity at a scale that is relevant to the life cycles of stream fishes.

Preface

This dissertation is the result of a field survey conducted at Carnation Creek designed in conjunction with my supervisor Marwan Hassan. The field data used for this research was collected with help from Dave Reid, Kyle Wlodarczyk and Ryan Matheson. Reference data on the study area was provided by the British Columbia provincial Ministry of Forests, Lands and Natural Resource Operations. A paper with Marwan Hassan as a co-author will be submitted for publication, based on material in Chapters 2 and 3. I completed all analysis and processing of the data.

Contents

List of Tables

List of Figures

List of Symbols

Symbol	Definition	Units
A	cross-sectional area	L^2
cm	centimetre	L
d	water depth	L
D	grain diameter	L
D_x	percentile of grain diameter	L
DEM	digital elevation model	-
g	acceleration due to gravity	$\mathrm{L\ T}^{-2}$
km	kilometre	L
l	longitudinal distance along channel	L
H	Shannon's diversity index	-
LiDAR	Light Detection And Ranging (Remote Sensing)	-
n	Manning's roughness coefficient	$\mathrm{T\ L}^{-\frac{1}{3}}$
n	number of samples	-
m	metre	L
p	proportion of channel type	-
P	wetted perimeter	L
PC1, PC2, and PC3	principal component axis 1, 2, and 3	-
PCA	principal component analysis	-
Q	discharge	$\mathrm{L}^3\ \mathrm{T}^{-1}$
Q_s	sediment flux	$\mathrm{m\ T}^{-1}$
R_h	hydraulic radius	L
r^2	coefficient of determination	-
SA	study section	-
S_l	local slope	-
S_{ws}	local slope of water surface	-
S_r	reach slope	-

t	time	T
RPA	remotely piloted aircraft	-
v	velocity	L T^{-1}
W	wetted channel width	L
z	bed elevation	L
ρ	density of water	m L^{-3}
τ	shear stress	m L^{-1} T^{-2}
τ^*	dimensionless shear stress	-
2D	two-dimensional	-
3D	three-dimensional	-

Acknowledgements

I would like to extend my sincere gratitude to my supervisor Marwan Hassan. Without his continual support, understanding and guidance I could not have completed this research. The wonderful people I have met, and projects I have been part of, have allowed me to learn and experience more both academically and personally than I could have anticipated, and I am grateful for his role in this.

I would also like to thank my lab-group and office mates for their encouragement and advice along the way, especially to Dave Reid for his support in teaching the necessary field skills and always sparing time to share his advice on the project and anything graduate-school related. To Steve Bird of Fluvial Systems Research, and my committee member John Richardson, I am grateful for the discussions we've had and insightful comments shared, which have helped to shape my research. Thank you to Brett Eaton as well for helping inspire my interest in fluvial geomorphology during my undergraduate studies and for continuing to provide advice on the RPA-related aspects of this research.

This project would not have been possible without the support of the British Columbia provincial Ministry of Forests Lands and Natural Resource Operations. Thank you to Peter Tschaplinksi and Robin Pike for their interest in this research, for sharing data and for helping facilitate the field work. To Steve Voller and Andrew Westerhof, many thanks for making our time at Carnation Creek so memorable and helping to ensure the smooth operation of the camp. I was very fortunate to be part of a great field crew for this research, and thank Kyle Wlodarczyk, Ryan Matheson, Kevin Pierce, Dave Reid, Dave Adams, and Jack Carrigan for their hard work in the field and positive attitudes.

Thank you to my parents, Charles and Linda Helm, for instilling my interest in the natural sciences from a young age and their unwavering love and support in my pursuits. Thank you to my brother Daniel, for always being available to take stressed phone calls and offer wise words of advice. Last but not least, thank you to my partner, Jack Carrigan for his patience, belief in me, and for helping me stay grounded throughout this process.

Chapter 1

Introduction

1.1 Background

Globally, wild salmon stocks are in decline. Their stressors are numerous, but their decline is often attributed in part to degradation of their freshwater habitat (*Nelson et al.*, 2015). To remedy this, millions of dollars are annually put into restoration programs to improve freshwater conditions (*Bisson et al.*, 2009). Despite this large investment, the declines and low rates of recovery in several stocks are still persistent, and may point to a broader misunderstanding of salmonids and their life requirements (*Fausch et al.*, 2002; *Bisson et al.*, 2009). This may be because of an emphasis on designing channels to contain what is considered to be ideal habitat, rather than restoring natural processes of the stream system itself. Pacific salmon have diverse life histories, so it is logical to assume that they are adapted and well-suited to the spatial and temporal diversity in habitat provided by the natural processes of stream systems (*Bisson et al.*, 2009). This is seen today by restoration frameworks that call for the reestablishment of natural processes in streams, rather than altering these systems to contain what is considered to be "good" habitat (*Beechie et al.*, 2010).

The neglect for restoring natural processes in previous conservation frameworks likely stems from prior conceptual theories that the ideal ecosystem is static and in equilibrium, which leads to the notion that disturbance should be discouraged (*Wallington et al.*, 2005). However, there has since been a shift in ecological thinking that celebrates the variability provided by the natural processes of stream systems and their capacity to provide an array of aquatic habitats. The 1990s and early 2000s saw the rise of many notable studies that encouraged the characterization of ecological processes in stream systems continuously and at a scale relevant to species' life histories (*Fausch et al.*, 2002; *Schlosser*, 1991). The "Riverscape Approach" to viewing aquatic habitat posited by *Fausch et al.* (2002), emphasizes heterogeneity in streams as a critical factor influencing stream fish distribution and structure, and has been observed in other studies (e.g. *White et al.*, 2008; *Kim and Lapointe*, 2011). The logic for this approach is evident when considering that fish complete their life cycles in streams at intermediate spatial scales between 1 and 100 kilometres in length (*Fausch et al.*, 2002). It therefore encourages characterization of streams at a scale relevant to these processes. However, this has been a scale that has traditionally been difficult to characterize.

The present understanding of streams has been well informed by studies conducted at both small scales (from the microhabitat and channel unit to reach extent) and large scales (basin extent). It is the intermediate scale that has been lacking and that requires more investigation (*Fausch et al.*, 2002). With advances in remote sensing technologies, it is becoming easier to survey this intermediate scale at high resolutions to address the gap between conceptual theories such as the "Riverscape Approach" and empirical observation. However, with the ability to collect high resolution and continuous data comes the challenge of translating it into a meaningful form that can aid stream scientists in understanding and managing these systems.

1.2 Classification of channel form

Classification schemes for characterizing channel morphology have held an important place in fluvial geomorphology to help understand and analyze the natural world. While the channel characteristics that they stem from, such as topography, grain size, and channel width and depth, are continuous variables, at the morphological unit scale they do appear to correspond with predictable channel controls. This can be observed in a recent study noting the influence of characteristic width gradients on pool-riffle formation (*Chartrand et al.*, 2018). Discernable morphologies, such as pools and riffles, can also provide functionally different habitat for aquatic species (e.g. *Bisson et al.*, 1988; *Flitcroft et al.*, 2012; *Naman et al.*, 2017). Therefore, classification of these channel types should provide a useful tool for investigating relationships between salmonids and their physical environment. Several classification schemes have been proposed that aid this goal (*Frissell et al.*, 1986; *Hawkins et al.*, 1993; *Rosgen*, 1994), each of which may be tailored to the environment they were developed in, thus limiting their broad-scale application (*Nestler et al.*, 2016). Furthermore, the use of these early classification schemes often requires qualitative and subjective decisions from the observer for which channel type to prescribe to a channel unit. Because quantitative relationships between channel characteristics and channel form exist, there should be an opportunity for an improved objective classification scheme to be developed.

Early geomorphologists qualitatively noted the relationship between channel characteristics and form through the Lane Balance (Equation 1.1) (*Lane*, 1955). Equation 1.1 reflects a balance between the slope (S), discharge (Q), sediment flux (Q_s) and grain size (D) in a channel under equilibrium conditions, as can be observed in nature.

$$D \ \alpha \ \frac{QS}{Q_s} \tag{1.1}$$

Fluvial geomorphologists have since developed relationships that explain the processes leading to a channel's form. Chief among them is the shear stress equation (Equation 1.2), which describes the force exerted by water on the bed, where water density (p) and gravity (g) are constants and depth (d) and slope (S) describe the channel's shape.

$$\tau = \rho g d S \tag{1.2}$$

Equation 1.3 elucidates how the channel slope, sediment characteristics and scale can inform a channel's sediment transport regime (described by the shields number - the non-dimensionalized shear stress) (*Church*, 2006). It can then be inferred that along a typical channel, the transport regime will change along with the slope and roughness of the channel. As demonstrated by *Tamminga* (2016), it is important to consider these relations to provide a better understanding of how a stream may adjust to channel conditions and how that will influence its morphology.

$$S = 1.65\,\tau^* \frac{D}{d} \tag{1.3}$$

With the channel characteristics noted above, there may be an opportunity to conduct an objective characterization of channel morphologies that builds on a quantitative understanding of these systems. As described above, there is a general theme for the prior equations to include the following channel properties: hydraulic geometry, slope, and grain size characteristics. Therefore, there is a theoretical basis for inclusion of these variables in a statistical classification of channel types that could be conducted on and therefore best suited to a particular region of interest. Development of such an objective and quantitative scheme is likely advantageous as it would protect against human pre-conceived notions of channel type, and may highlight patterns that would otherwise be missed in a visual classification.

1.3 Application of remotely piloted aircrafts and classification schemes to small streams

The use of remotely piloted aircrafts (RPAs) (e.g. *Tamminga*, 2016; *Dietrich*, 2017; *Woodget and Austrums*, 2017) and efforts to objectively classify channel morphology at large spatial scales (*Lindenschmidt and Long*, 2013; *Hugue et al.*, 2016) have both become emerging research themes in fluvial geomorphology. However, the use of RPAs for studying riverscapes has been limited in the types of environmental conditions it has been applied to. The environments in which they have been tested in can be divided into two broad categories:

- Segments of larger channels (e.g. *MacVicar et al.*, 2009; *Tamminga*, 2016).
- Small streams lacking a dense riparian canopy (e.g. *Woodget and Austrums*, 2017)

It appears that application of this tool to small, forested mountain channels is lacking. Yet the ecological importance of these streams cannot be understated, and is seen by the high numbers of salmonid species such as cutthroat trout and coho salmon that reside in these systems (*Rosenfeld et al.*, 2000). It has been postulated that several unique characteristics of small streams may have led to this preference, including that the influence of large wood on providing complex habitats is most effective in small, gravel-cobble bedded streams (*Rosenfeld et al.*, 2000). This suggests that despite their small size, these streams are morphologically unique and can provide important habitat for salmonids. They also comprise a significant portion of the channel network and are often degraded by industrial, urban and agricultural activities (*Rosenfeld et al.*, 2000). Acknowledgement of this can be seen by the efforts in the 1970s to construct a long-running study at Carnation Creek to assess the influence of logging treatments on ecological and geomorphological processes (see *Tschaplinski and Pike*, 2017). Results of the study show that forestry can have long-term impacts on habitat, through changing the temperature regime of the channel to changing sedimentological processes (*Tschaplinski and Pike*, 2017). In conclusion, not only are the dynamics of small stream systems unique, but these systems can also be severely influenced by watershed management decisions, thus highlighting the need to provide observations that can inform protection of these systems.

Despite a need to better understand small, forested stream systems, it appears that efforts to survey them have not kept pace with remote sensing techniques seen in other stream systems, likely because dense canopies often make viewing them from aerial platforms a challenge. However, with the greater maneuverability and availability of RPAs, there may be an opportunity to bring modern techniques to the surveying of small, forested channels. Given the importance of small, forested streams in providing aquatic habitat to fish species, improving field techniques and classification schemes in this environment may be beneficial. With the advent of RPA technology there may lie an opportunity to more easily acquire data at the basin-scale to link patterns in ecological and geomorphological processes in these systems. To further this goal, the objective of this research is to provide a means of rapidly and objectively surveying and classifying small, forested stream systems to better inform their management. This objective was investigated through answering the following research questions:

- How can RPAs be used to characterize channel characteristics of a small, forested channel at the basin-scale using a sub-canopy survey?
- How can continuous measurements of channel characteristics be used to rapidly and objectively characterize patterns in channel morphology?
- What metrics can be used to characterize patterns in channel diversity, and what is the necessary scale to study these systems for watershed management?

These research goals are addressed over two chapters of this thesis. The first chapter provides an overview of the new technique employed to survey a small, forested mountain channel and of how relevant channel features were extracted. The second chapter investigates how these features can be used to objectively and near-continuously characterize patterns in channel morphology, and provides some of the basin-scale conclusions that can be drawn from the data.

Chapter 2

Sub-canopy, remotely piloted aircraft survey of channel features in a small, forested mountain channel

2.1 Introduction

The use of RPAs in fluvial geomorphology has become well established in the last decade with applications ranging from inventory of channel features to hydrodynamic flow modelling of streams (e.g. *Tamminga*, 2016; *Woodget and Austrums*, 2017). To date, the use of RPAs in such studies has several features in common. They are generally conducted on smaller segments of the larger stream network and are limited to channels with ideal survey conditions, where the streambed can be clearly viewed from a RPA flying above the forest canopy. Such conditions are not commonly found in small, forested mountain channels that are common in the Pacific Northwest. The temperate rainforest that these channels reside in often results in the forest canopy blocking observations of the channel bed and banks from RPA imagery collected above the forest canopy. While these channels compose a significant portion of the channel network in the Pacific Northwest and provide important habitat for many salmonids, it has remained a challenge to characterize them using techniques that larger streams have benefited from.

The difficult terrain imposed by streams makes ground surveys of channel morphology a demanding and time-consuming task, resulting in such surveys often being conducted in short segments of a channel. Similarly, traditional methods of estimating sediment texture involve a significant field component and are not well suited to surveying large areas frequently. Because of the human resources required, these methods are at odds with the argument that it is better to attain coarser data on aquatic habitat at a scale relevant to aquatic processes than detailed data at the wrong scale (*Fausch et al.*, 2002). While imagery from airplane and satellite platforms has provided an excellent method for landscape classification, its applicability has been limited to environments such as those that lack riparian vegetation (in arid or cleared agricultural environments) or wide streams with minimal riparian vegetation in dense forested environments. Furthermore, these platforms are often limited in their ability to map sediment texture due to their lower spatial resolution. Similarly, LiDAR has proven successful in habitat studies such as large wood (LW) identification (see *Abalharth et al.*, 2015), but the method is often costly for commercial use. Furthermore, unless green band LiDAR is used in conjunction with infrared LiDAR, the bathymetry cannot be mapped, which makes this tool ineffective for characterizing the submerged bed (*Muste et al.*, 2012). In contrast, RPAs are becoming increasingly affordable and flight paths can be user-defined to meet the unique needs of a study, but their use has also been limited to studies under ideal environmental conditions.

Challenges in employing sub-canopy surveys may stem from the fact that image acquisition for RPA-surveys often involves using vertical images (images taken where the camera lens axis is perpendicular to the ground) with parallel flight paths to characterize an area, as has been traditionally employed in airplane surveys for the last several decades (*James and Robson*, 2014). However, the techniques used for traditional photogrammetry differ from those employed in structure-from-motion (SFM) based photogrammetry, which may allow for development of flight paths better suited to a sub-canopy survey. For traditional photogrammetry, metric cameras with known internal camera geometries and lens distortions are used in combination with two overlapping photos of known position and distance from one another, to establish distances from the camera to features in the imagery (*Dietrich*, 2014). With SFM-based photogrammetry, common features are identified in multiple images to reconstruct the geometry of a site from which arbitrary camera positions and orientations are generated automatically. This approach allows non-metric cameras to be used and the freedom to collect images from a range of unknown positions and orientations.

Recently, there has been greater emphasis on testing flight patterns that deviate from those used in traditional photogrammetry. Perhaps the most notable finding is the positive effect incorporation of oblique and highly convergent imagery can have on overcoming errors introduced from the non-metric cameras frequently used in RPA-surveys (*Wackrow and Chandler*, 2011; *James and Robson*, 2014; *Harwin et al.*, 2015). Non-metric cameras are light and less costly than their metric counterparts, but are prone to greater distortions as they are manufactured to a lower standard (*Harwin et al.*, 2015). While this can be overcome by a self-calibration of the camera in the SFM software, the incorporation of oblique-convergent imagery has been shown to minimize systematic errors in model outputs that often plague projects where only imagery with a vertical orientation is employed (*Harwin et al.*, 2015).

Through embracing these findings, there may be an opportunity to overcome the survey challenges imposed by small, forested stream systems. Oblique imagery is likely advantageous in streams where riparian vegetation may prevent the RPA from flying directly over the bank. In this situation it may be possible to characterize these obstructed portions of the channel through oblique and convergent imagery originating from a clear flight path below the canopy. However, few studies to date provide guidelines for RPA-surveys conducted below the canopy to characterize small, forested stream systems. This work seeks to provide a framework for characterizing channel features in these systems and a first assessment of the accuracy and coverage that can be acquired when employing RPAs in this new environment. To build this framework, this chapter aims to meet three objectives:

- Investigate the influence of low elevation oblique-convergent imagery on the accuracy of model outputs.
- Discuss techniques to filter overhanging vegetation that plagues models in these systems and tools for extracting channel features such as bathymetry, sediment texture and large wood.
- Evaluate the method against traditional total station survey data collected in the channel.

2.2 Methods

2.2.1 Study area

Carnation Creek is a small gravel bed stream located on the southwest coast of Vancouver Island (Figure 2.1). The watershed it resides in has been the site of a long-running, fish-forestry interactions study, initiated in the 1970s, to assess the impact of different logging treatments on the watershed. The stream is ∼8 km long and has a drainage area of ∼11 km^2 (*Tschaplinski and Pike*, 2017).

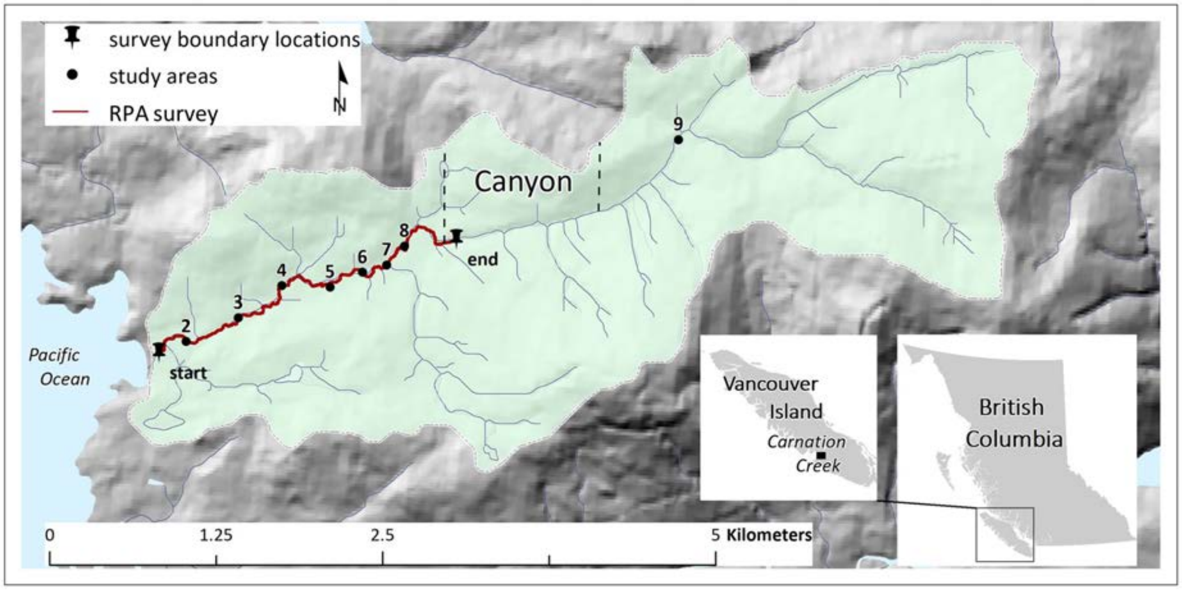

Figure 2.1: The Carnation Creek watershed, located on the south-west coast of Vancouver Island. The start and end points of the RPA-survey are indicated on the map as thumbnails, as well as the midpoints of the eight geomorphology study sections (SAs 2–9). Initially study section one was established in the estuary, but has since been abandoned and was not included in the survey. Coordinate system is NAD83 UTM Zone 10.

The watershed bears evidence of its glacial history through a stepped longitudinal profile with alternating segments of mild and steep gradients (*Reid et al.*, 2019), as is characteristic of deglaciated systems (*Brardinoni and Hassan*, 2007). The first approximately 3 km of the channel are mildly sloped and dominated by riffle-pool morphologies, after which the channel narrows into a canyon that sees the onset of step-pool morphologies and provides a barrier to fish passage (*Reid et al.*, 2019). The average bankfull width of the lower channel is approximately 15 m and the sediment texture of the bed varies from small gravels near the mouth of the channel to coarser cobbles and boulders as the canyon is approached (*Reid et al.*, 2019). Anadromous salmon that inhabit the lower 3 km of channel include coho salmon (*Oncorhynchus kisutch*), chum salmon (*Oncorhynchus keta*), rainbow trout (*Oncorhynchus mykiss*) and cutthroat trout (*Oncorhynchus clarki*) (*Tschaplinski and Pike*, 2017).

Detailed channel morphology data have been collected through annual total station surveys in eight study sections (SAs 2–9), seven of which are located downstream of the canyon (SAs 2–8) (Figure 2.1). Initially a study section was established in the estuary (SA1) however, the site has since been abandoned and was not covered for this research. The most upstream study section is study section nine, which is located above the canyon. The lower study sections are 300–500 m apart and 5–10 bankfull widths in length (*Reid et al.*, 2019).

The channel is located within the Coastal Western Hemlock Biogeoclimatic Zone of

British Columbia (CWH) (*Hartman et al.*, 1982). Western hemlock is the most common tree species of the CWH, followed by red cedar and Douglas-fir (*Pojar et al.*, 1991). In logged areas, red alder is common and widespread (*Pojar et al.*, 1991). As illustrated in Figure 2.2, much of the channel is hidden below a dense forest canopy composed of both coniferous and deciduous tree species. In order to characterize the majority of the channel bed it would therefore be necessary to fly the RPA below the forest canopy. In July of 2018, approximately 3.5 km of the channel was surveyed from the mouth of the channel to the beginning of the canyon, as well as the lower half of SA9, over a period of ten days.

Figure 2.2: (a) Google Earth satellite imagery of Carnation Creek (Map data ©Google 2019, Maxar Technologies), showing the topography of the site, midpoints of study sections two through eight, and location of the channel in yellow. (b) Canopy coverage in a section of the channel upstream of a weir with a cable car that provides a relatively clear view of the channel bed. (c) Nearly closed canopy coverage that partially obstructs view of the bed, as is typical throughout the channel. Note that (b) and (c) were taken from an aircraft after fall, which differ from the summer conditions present during the RPA-survey where the presence of leaves led to more pronounced canopy coverage.

2.2.2 Remotely piloted aircraft survey

The RPA-survey involved low-level flights conducted in tandem with placement of surveyed Ground Control Points (GCPs). The RPA-survey was conducted using the DJI Phantom 4 Advanced, which contains a camera with a focal length of 8.8 mm (24 mm in 35 mm format equivalent) and a field of view of 84°. To remove the influence of the forest canopy obstructing view of the channel, the RPA was flown manually below the canopy, which resulted in flying heights ranging from approximately 3–15 m above ground level. Channel segments were chosen that split the channel into approximately straight sections that were 40–60 m long and bounded by areas with rough terrain (e.g. channel-spanning log jams). These segments provided manageable blocks along the channel to navigate with the RPA, and would comprise individual photosets for image processing. The images were acquired in automatic mode to mitigate the influence of changing lighting conditions along the channel and at a capture rate of a photo every 2 s while moving at approximately 1 m/s to attain maximum overlap between photos. In total, the approximately 3 km of surveyed channel was broken into approximately 80 segments with 300–1000 photos each.

Each channel segment was initially flown with a traditional flight path consisting of parallel flight lines with vertical imagery while striving to attain at least 60% side and forward overlap, as has been noted as convention in other studies (*Ortega-Terol et al.*, 2014). The reach was then flown with oblique and convergent imagery, with an emphasis on ensuring that the channel banks were well covered. To do this the camera was tilted at a low-oblique angle (20–30° from vertical, see Figure 2.3a) and a flight path as shown in Figure 2.3b was employed. As illustrated, the RPA was first flown parallel to the bank with the camera oriented in an upstream direction, and then the path was repeated with the camera orientated in a downstream direction to acquire oblique-convergent imagery. These steps were completed at multiple distances from the bank to ensure sufficient overlap with the vertical photosets.

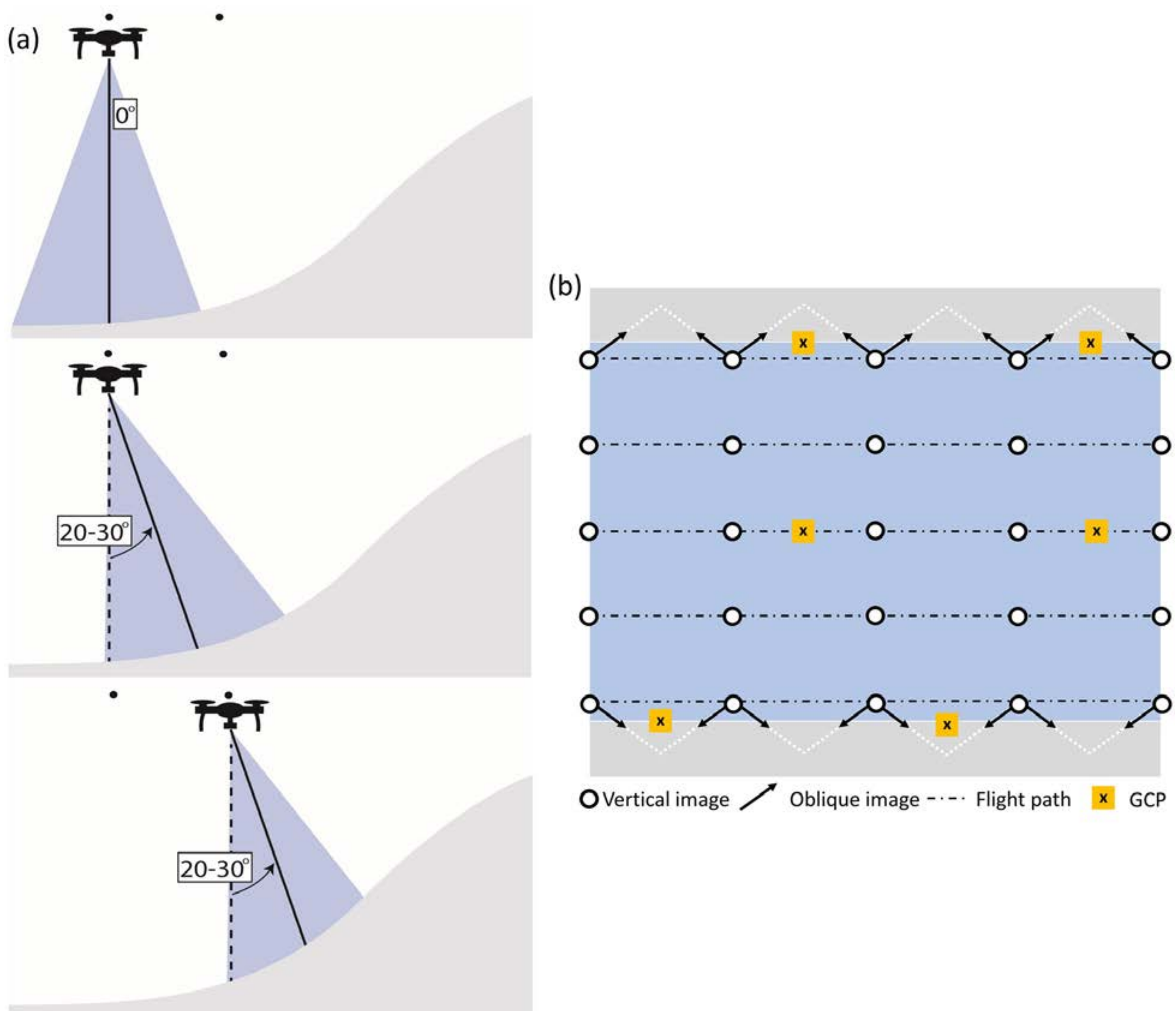

Figure 2.3: (a) Channel cross section showing the oblique angles of the RPA's camera (indicated by the solid black line) for image acquisition of the banks. To characterize the channel banks, the camera was tilted 20–30° from vertical. (b) Plan view of the flight path of the RPA with the parallel flight lines shown as dashed lines. The outlined circles show the locations of a vertical image, and the arrows show the horizontal orientation of the camera towards the channel banks for the oblique images described in (a)

We aimed to spread at least ten GCPs across each reach to georeference the imagery, with the remainder serving as checkpoints to assess the accuracy of the model outputs. The majority of the GCPs were distributed in a zig-zag fashion along dry exposed bars in the periphery of the reaches, with a smaller number situated towards the centre. While there does not appear to be a universally accepted number or distribution of GCPs required for optimal model outputs at the time of writing (see *Sanz-Ablanedo et al.*, 2018), this set up was a balance between findings in the literature that suggest using between 4–15 GCPs with distributions either purely in the periphery, periphery with the addition of central points, or uniformly across a site (*Harwin et al.*, 2015; *Agüera-Vega et al.*, 2016; *Tonkin and Midgley*, 2016; *Sanz-Ablanedo et al.*, 2018). Each GCP consisted of an orange 10 cm x 10 cm ceramic tile with a central X marking the surveyed location. The location of the GCPs were measured using a Leica TPS 1100 total station through a local survey that included shots of well-established benchmarks in the study sections. These benchmarks were then used to transform the coordinates into the projected coordinate system NAD83 UTM Zone 10 by applying an affine transformation through an in-house script and the package 'vec2dtransf' in R (*Carrillo*, 2014).

2.2.3 Photogrammetry

Agisoft PhotoScan general workflow

The software Agisoft PhotoScan Professional (version 1.4.3) was used to generate dense point clouds of each reach. These are 3D point clouds of the reach, containing millions of points that are built from the matched points in the photoset (*Henry*, 2018). The steps it employs to do this include aligning the photos through matching features across images, and performing a bundle block adjustment in an arbitrary coordinate system that leads to the formation of a sparse point cloud (*Mayer and Kersten*, 2018). The addition of GCPs for georeferencing the model allows for this adjustment to be further optimized, which refines the camera calibration. This can be an important step in mitigating the effect of systematic errors in the model output derived from non-metric cameras. Following this a dense point cloud of the optimized sparse cloud can be created. The incorporation of these steps in the workflow is outlined in greater detail below.

Application to channel survey data

For this analysis, the Estimate Image Quality function in PhotoScan was first used to identify low quality images, which were then visually assessed to identify blurry photos for removal. Due to erroneous location measurements by the RPA's on-board GPS, the image coordinates were cleared prior to alignment. The erroneous measurements mostly occurred early on in the flights, suggesting that the GPS had not yet connected to a suitable number of satellites for accurate positioning prior to the beginning of some flights. The photos were then aligned using medium accuracy, a key point limit of 40,000 and tie point limit of 2,000. A low density point cloud was then generated to allow the GCPs to be easily identifiable. GCPs were then selected on the point cloud and the appropriate coordinates were attributed to their position in the photos. After updating the model, image residuals for the GCPs and tie points were viewed and adjusted in the reference pane as suggested by *James et al.* (2017) to ensure that they would not be weighted too heavily in the optimization. Then the camera positions were optimized with the GCPs selected to refine the camera calibration, leading to the generation of a re-adjusted sparse point cloud. The final dense point cloud was then generated under medium quality and with aggressive depth filtering. This workflow was repeated for each reach to generate dense point clouds across the entire study area. Setting the accuracy of the photo alignment and dense point cloud quality to medium was deemed a suitable balance between processing time and representative model outputs.

2.2.4 Dense point cloud cleaning

The open source software Cloud Compare (version 2.1) was used to further clean the point clouds. To remove the influence of vegetation obstructing bed points, the Cloth Simulation Filter (*Zhang et al.*, 2016) was applied to the clouds. Initially developed for processing of LiDAR point clouds, this tool has rarely been applied to RPA derived point clouds in previously published studies, despite evidence suggesting its high performance relative to other ground filtering algorithms (*Yilmaz et al.*, 2017). Incorporation of this tool may allow RPAs to overcome drawbacks noted by *Tamminga et al.* (2015), namely their explicit suitability to streams with wide active channels where trees minimally obscure view of the channels. To remove the influence of riparian vegetation, the tool inverts the point cloud and 'drapes' a simulated cloth (*Zhang et al.*, 2016) over the inverted surface to approximate the terrain of an area. The resolution of the cloth, and the maximum distance a point may be from the cloud to still be considered part of the ground surface, can be altered to best suit the environmental conditions. Setting the cloth resolution to a value of 0.1 m and maximum distance between 0.5–1.0 m was found to adequately filter the bed points.

2.2.5 Water depth corrections

Point clouds generated from SFM suffer from the effect of refraction causing submerged bed elevations to be over-estimated. To correct for this and develop bathymetry maps of the channel, a script developed by *Dietrich* (2017) was used. A requirement of this script is clear water allowing the channel bed to be viewed. During the study period, few opaque or turbulent wetted channel areas were present due to low flow conditions, though a polarizing filter was also fitted to the drone to mitigate the influence of surface reflections on the water surface.

The method requires a water surface mesh to be delineated across the channel. By determining the distance from the mesh to the SFM bed elevations below, the corrected water depth for a location on the bed can be calculated as a function of the multiple viewing angles used to observe the location and through the application of a correction factor. Prior to running the script, the clouds were sub-sampled to a spacing of 2 cm while retaining the minimum height in each cell to further clean the clouds and ensure anomalous points from overhanging vegetation were removed in Cloud Compare. For more details on the application of this method, and how the input files were generated, see *Dietrich* (2017). Following the correction, the uncorrected point clouds of the entire channel and corrected point clouds for the wetted area were then transformed into 2 cm resolution Digital Elevation Models (DEMs). These were merged together so that overlapping areas only retained the corrected bed elevations. The corrected water depths were also extracted from the submerged point clouds to create bathymetry rasters across the channel.

2.2.6 Sediment texture analysis

Grain size estimates of the exposed bed were acquired through establishing a relationship between the roughness of the point cloud and the D_{50} and D_{84} of 22 field training sites across the channel (*Woodget and Austrums*, 2017). Each field site was ∼1 m x 1 m and was photographed by hovering the RPA ∼2 m above ground level. Using an in-house photo-sieving GUI in Matlab the grain size distributions of each training site was determined. First the photos of each site were scaled based on the known diamter of the GCPs in the images. Then a 10x5 grid was overlaid on the photos, which allowed the b-axis of the 50 particles that fell below the grid nodes to be measured for calculation of each site's grain size distribution.

The roughness of each point in the point clouds was determined by using the 'roughness tool' in Cloud Compare. This tool computes the roughness of each point relative to the distance from the point to an ordinary least squares plane, fitted through the point and its user specified neighbourhood. Prior to using this tool, areas of the cloud that did not contain bed material (e.g. log jams or vegetated banks) were removed. Then the tool was run with a specified neighborhood of 40 cm. As found by *Woodget and Austrums* (2017), this neighborhood size appeared to provide a good balance between ensuring that the largest clasts in the channel would be encompassed by the window and ensuring that the neighborhood was likely to contain homogeneous material. Following the roughness calculation, the training sites were extracted from the roughness clouds and exported as 2 cm rasters from which the mean roughness value for each raster was determined.

A linear model was then fit between both the D_{50} and D_{84} (Figure 2.4) of the training sites against their mean roughness value. The equation of this line was then used to estimate grain sizes across the entire channel. This was achieved in R by running a moving window of 1 m x 1 m across the roughness rasters. The mean roughness value for each window was determined and its centre cell replaced with the estimated grain size based on the predictive relationship (Equation 2.1), where D_{50p} is the predicted grain size for the centre cell of the window and R_w is the average roughness value of the cells in the window.

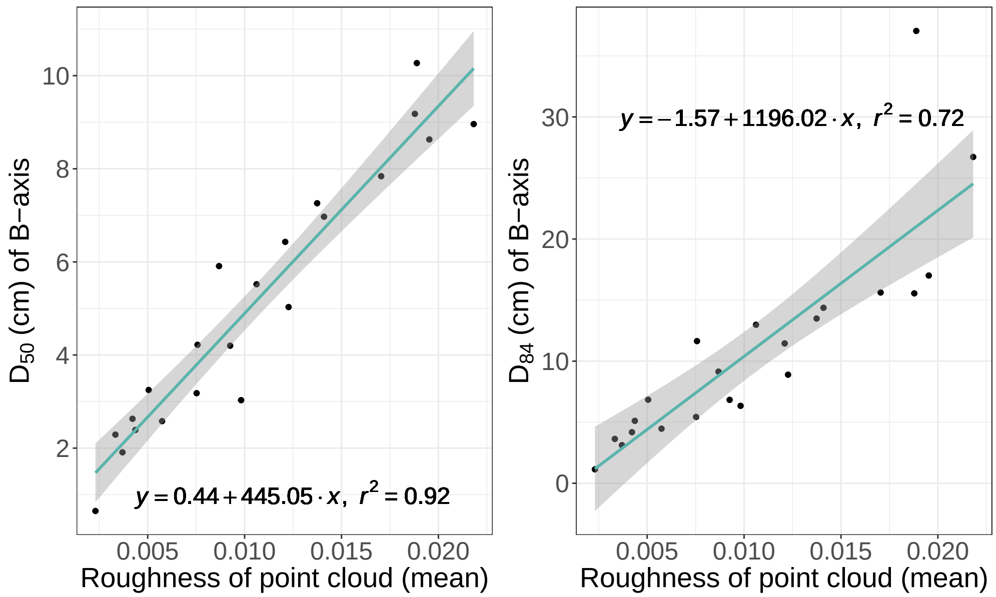

Figure 2.4: Predictive grain size relationships between a given grain size (D_x) and the average roughness value of the training sites.

$$D_{50p} = 0.44 + 445.05 \; R_w \tag{2.1}$$

2.2.7 Large wood extraction

Large wood is an important variable to consider in aquatic habitat delineations as it can provide both channel complexity and cover for aquatic species. Large wood was manually digitized across the channel and the area of each piece calculated using the DEMs and orthomosaics in ArcMap (version 10.6.1). Pieces of wood (larger than approximately 10 cm in diameter and 1 m in length), that appeared to be exerting a control on channel form were digitized individually, whereas log jams were digitized as polygons.

2.3 Results

2.3.1 Accuracy assessment

Remotely piloted aircraft survey

A detailed assessment of the accuracy and reproducibility of the sub-canopy RPA results was undertaken to determine the suitability of the technique. To do this, a small reach was chosen early on in the photogrammetric processes that included the use of vertical and intensive oblique imagery to characterize the banks. The reach was chosen as it was relatively small for repeat processing (approximately 30 m in length and 10 m in width) and because the presence of overhanging vegetation (Figure 2.5) made it a challenging reach to survey that was representative of difficult portions of the channel. As shown in Table 2.1, a greater number of photos included in the photoset was associated with a much greater time required to generate the dense point cloud.

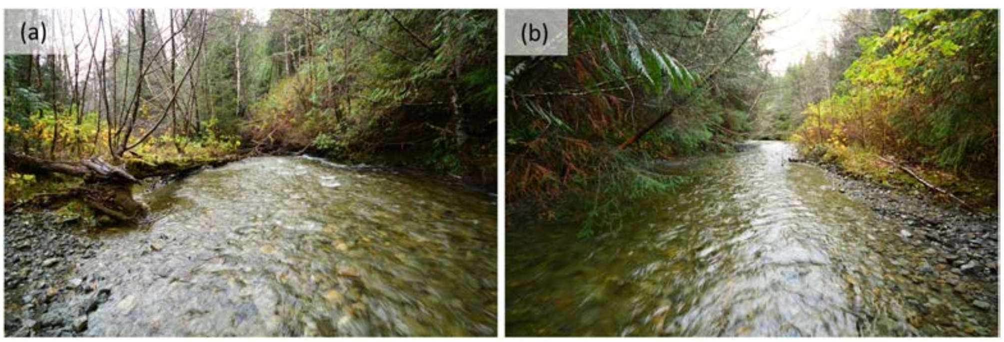

Figure 2.5: (a) Downstream view to a log jam at the beginning of the study reach. (b) Upstream view showing the presence of deciduous branches and overhanging vegetation that would require the RPA flight be low altitude and include oblique imagery. Note that the images were taken during the fall total station survey, and therefore the water levels are higher and leaf cover is lower than it was during the summer RPA-survey. Photos courtesy of Iain Reid.

Table 2.1: Computer processing time required for each photoset and GCP combination in PhotoScan.

	Photo matching	**Photo alignment**	**Depth map generation**	**Dense cloud generation**	**Total time**	**Number of photos**	**Number of points in cloud**
p1t1	13min 15s	5min 46s	35min 47s	3h 6min	∼4h	592	26,015,291
p2t1	4min 3s	2min 27s	8min 19s	30min 31s	∼45min	311	21,252,408
p3t1	3min 42s	3min 29s	8min 24s	25min 52s	∼40min	293	21,063,688
p4t1	5min 41s	1min 3s	18min 3s	9min 5s	∼35min	234	17,616,174
p1t2	13min 15s	5min 46s	36min 58s	3h 46min	∼4h	592	26,092,604
p2t2	4min 03s	2min 27s	8min 15s	29min 43s	∼45min	311	21,243,270
p3t2	3min 42s	3min 29s	8min 1s	24min 57s	∼40min	293	21,195,514
p4t2	5min 41s	1min 03s	17min 53s	9min 02s	∼35min	234	17,531,918
p1t3	13min 15s	5min 46s	36min 45s	3hr 5min	∼4h	592	29,941,363
p2t3	4min 03s	2min 27s	9min 07s	29min 37s	∼45min	311	21,311,393
p3t3	3min 42s	3min 29s	8min 01s	23min 29s	∼40min	293	20,824,947
p4t3	5min 41s	1min 03s	17min 45s	9min 03s	∼35min	234	17,608,597

Four combinations of photos were used, along with three combinations of GCPs as outlined in Table 2.2 and Figure 2.6, giving rise to twelve combinations of GCPs and photosets that were run through PhotoScan to generate DEMs of the site. Using only odd or evenly numbered photographs would allow for the creation of DEMs using two entirely unique photosets, that allow for an assessment of the reproducibility of the model outputs.

Table 2.2: Photoset and ground control point (GCP) and check point (CP) combinations.

Modifier	***Description***
p1	all photos
p2	odd photos
p3	even photos
p4	vertical photos only
t1	11 GCPs and 11 CPs
t2	5 edge GCPS and 17 CPs
t3	5 edge GCPs, 3 centre GCPs and 14 CPs

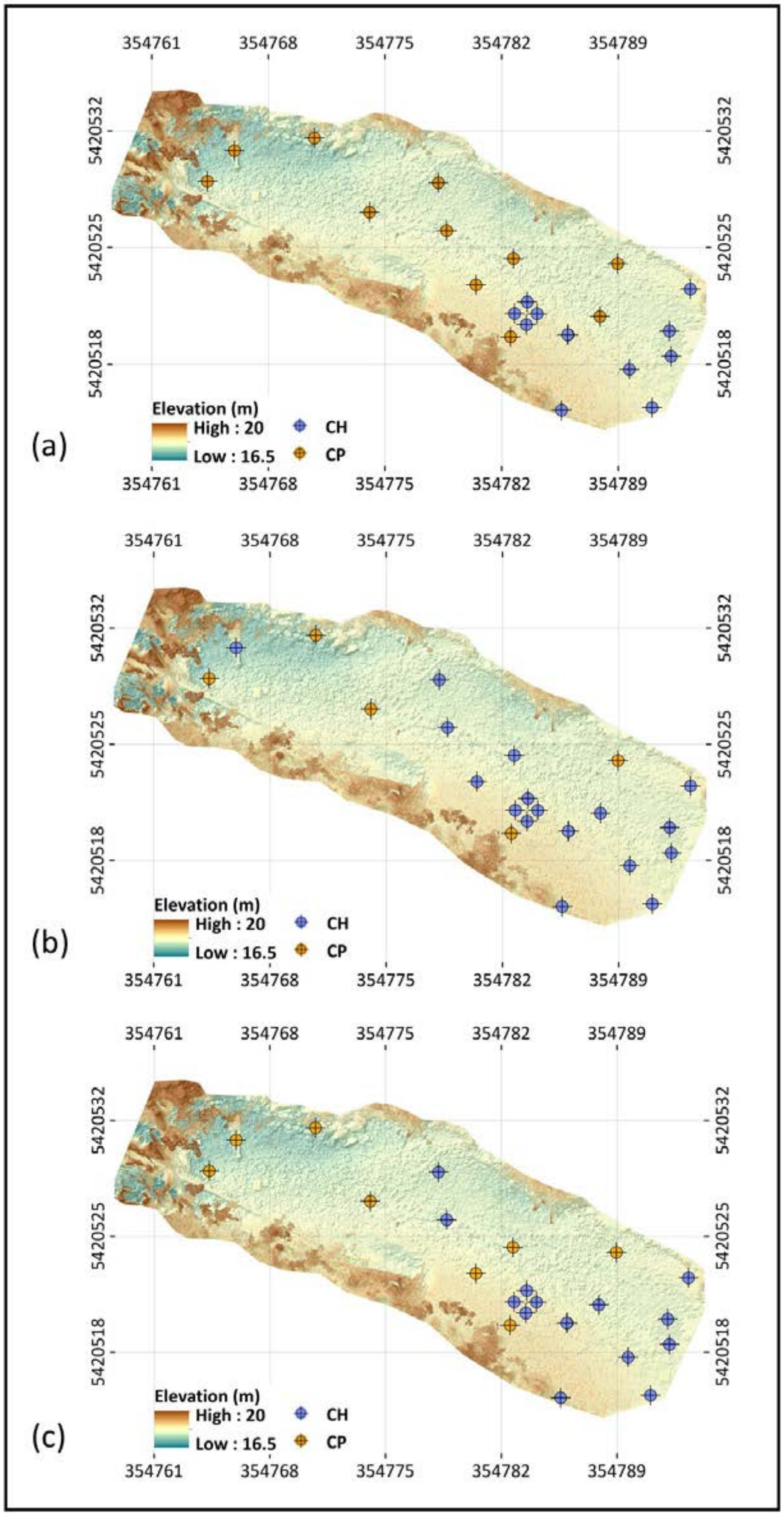

Figure 2.6: (a) Ground control point (CP) and check point (CH) distribution for modifier t1.(b) Ground control point (CP) and check point distribution (CH) for modifier t2.(c) Ground control point (CP) and check point (CH) distribution for modifier t3. Coordinate system is NAD83 UTM Zone 10.

Following this, the difference between the estimated elevations from each DEM and the actual elevations for the GCPs and CPs measured using the total station was determined. As seen in Figure 2.7, the majority of the errors for all models was within 2 cm, suggesting that the choice of flight path and GCP configuration had a small influence on the error. This was further confirmed by plotting the values from each DEM against one another to calculate their correlation coefficients (Table 2.3), which showed strong correlation between all DEMs regardless of the combination used. The difference in the proportion of channel that could be captured with the incorporation of oblique imagery, in contrast to the photosets where only vertical images were used, can be visually compared in Figure 2.8.

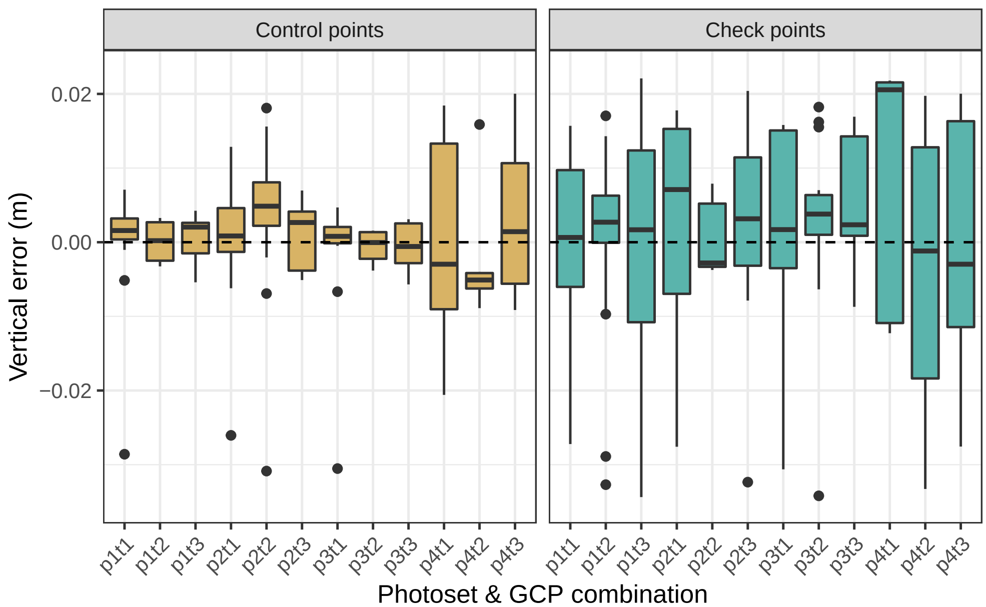

Figure 2.7: Boxplots showing the distribution of vertical error for the GCPs and CPs of each accuracy assessment. The boxes represent the interquartile range (IQR) and the solid black lines represent the median error for each photoset and GCP combination. The vertical whiskers represent the extent of the smallest and largest errors within 1.5 times the IQR below the 25th (Q1) or above the 75th (Q3) percentile, respectively. The dashed horizontal line represents a vertical error of 0. The dots are outliers which are either less than Q1 - 1.5*IQR or greater than Q3 + 1.5*IQR.

Table 2.3: Correlation matrix describing the similarity of the rasters (through their correlation coefficients) generated for all twelve unique GCP and photoset combinations.

	p1t2	**p1t3**	**p2t1**	**p2t2**	**p2t3**	**p3t1**	**p3t2**	**p3t3**	**p4t1**	**p4t2**	**p4t3**
p1t1	0.992	0.992	0.987	0.987	0.987	0.986	0.987	0.987	0.986	0.956	0.958
p1t2		0.997	0.991	0.993	0.992	0.99	0.992	0.991	0.991	0.959	0.962
p1t3			0.99	0.993	0.992	0.989	0.991	0.99	0.991	0.958	0.961
p2t1				0.99	0.994	0.988	0.989	0.989	0.987	0.956	0.958
p2t2					0.991	0.986	0.989	0.988	0.987	0.954	0.956
p2t3						0.988	0.99	0.989	0.987	0.957	0.959
p3t1							0.992	0.994	0.986	0.958	0.96
p3t2								0.994	0.987	0.958	0.96
p3t3									0.988	0.958	0.96
p4t1										0.963	0.966
p4t2											0.983

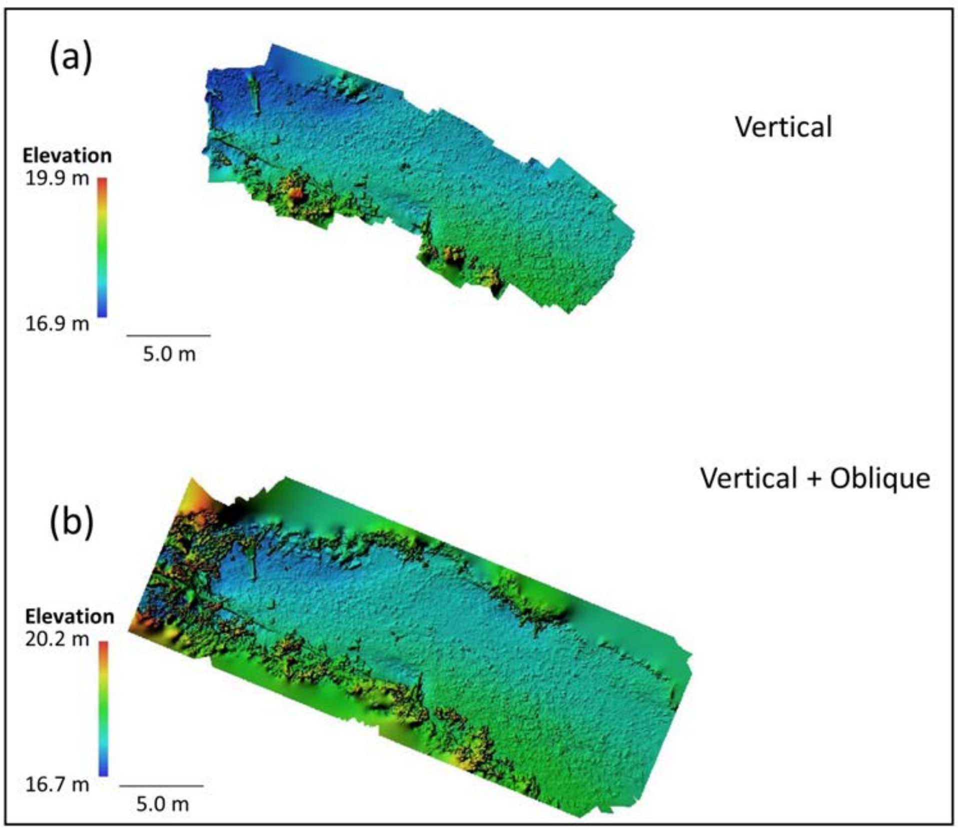

Figure 2.8: Difference in the proportion of bed that can be covered between only a vertical image photoset (a) and the incorporation of oblique images (b). The DEM with both vertical and oblique imagery (b) has more well defined channel banks as seen by the channel roughness provided by bank vegetation towards the margins of the channel.

The vertical error throughout the entire channel was estimated by comparing the elevations of check points not used for georeferencing the models to the elevations estimated by the DEMs. In total, 1724 checkpoints were spread across the channel, 1203 of which were located on the exposed bed and 521 of which were submerged below the water surface. The metrics used to characterize the vertical error in the models were the root-mean-square-error (RMSE) and the mean error (ME). The RMSE provides a measure of the spread of the squared residuals (Equation 2.2) whereas the ME provides a measure of any potential positive or negative bias to the data (Equation 2.3). These values were chosen as they provide comparable metrics to other accuracy assessments of RPA-surveys completed in the literature (e.g. *Tamminga*, 2016). The RMSE of the exposed bed points was found to be 0.093 m and 0.025 m for the ME (n = 1203), whereas for the submerged bed points the RMSE and ME was 0.1 m and 0.025 m (n = 521), respectively. The overall spread of this error is illustrated in Figure 2.9.

$$RMSE = \sqrt{\frac{\sum_i^n (z_{mod} - z_{obs})^2}{n}} \tag{2.2}$$

$$ME = \frac{\sum_i^n (z_{mod} - z_{obs})}{n} \tag{2.3}$$

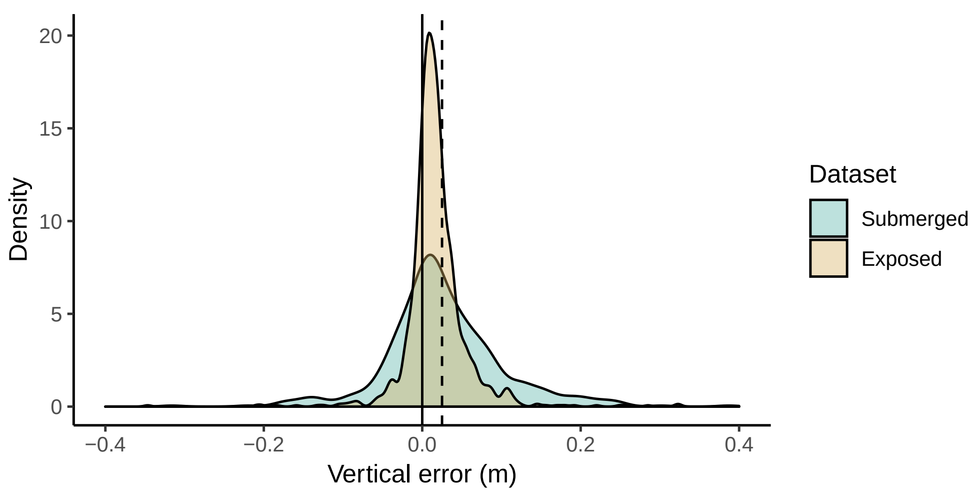

Figure 2.9: Density plot showing the distribution of vertical errors between the modelled and total station measured elevations. The dashed line represents the mean error for the datasets, and the solid line a vertical error of 0 m.

Bathymetry analysis

To assess the accuracy of the corrected submerged bed elevations, two locations were chosen in the channel where dense measurements of the bed were collected using the total station (Figure 2.10). The values from the uncorrected and corrected DEMs were compared to these true values as seen in Figures 2.11 and 2.12. Prior to the correction, these values deviated from the 1:1 line due to the influence of refraction, with the deviation greater at larger water depths. Following the correction, the observations plot along the 1:1 line, indicating that the corrections were successful.

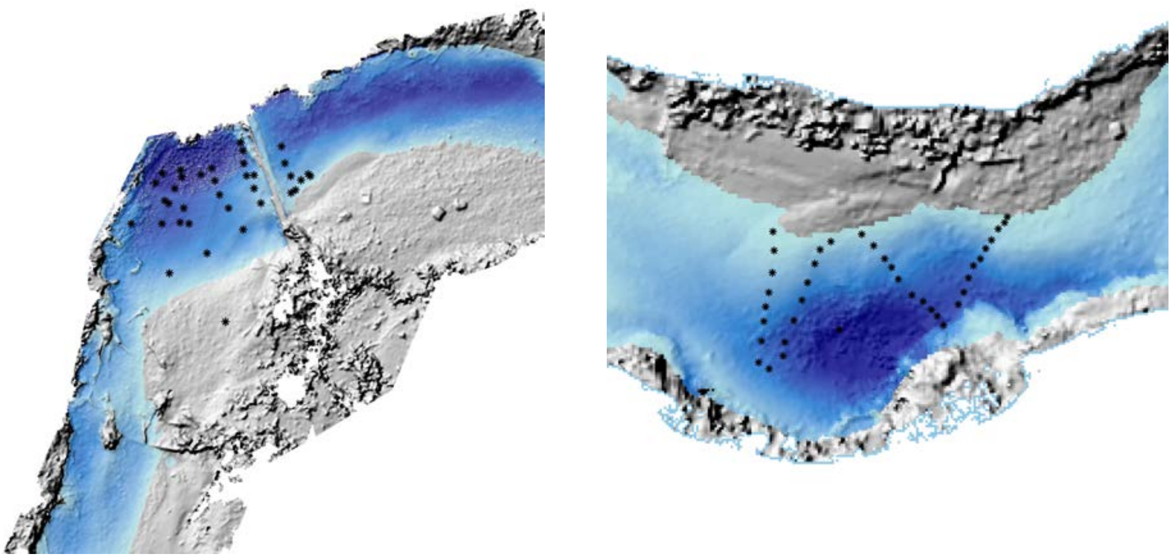

(a) (b)

Figure 2.10: Distribution of GCPs for the accuracy assessment of the bathymetry correction at sites (a) and (b).The bed texture is displayed through a hillshade layer, with smoother textures corresponding with finer material, and very rough textures towards the margins of the channel corresponding with vegetated areas. The extent of the water surface is indicated in blue, with darker blues corresponding with deeper sections of the channel.

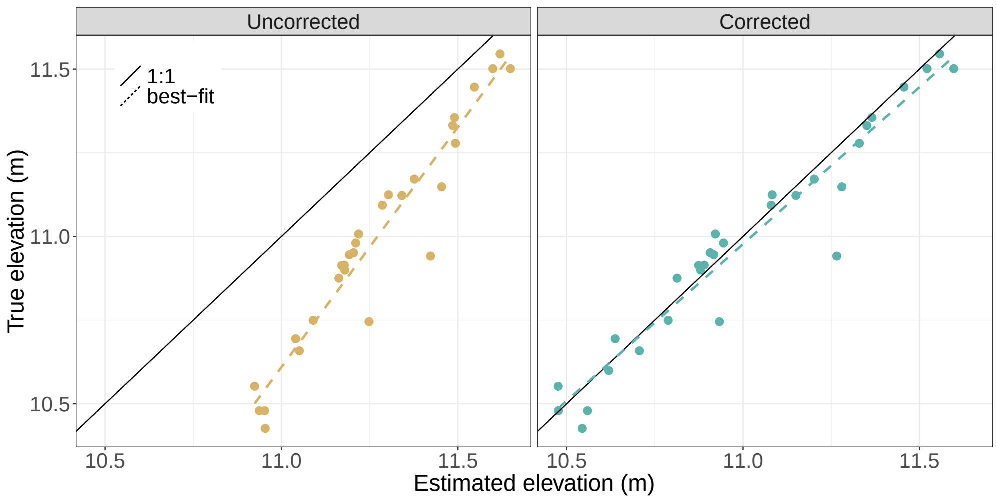

Figure 2.11: Comparison of the submerged bed elevations to the total station measured elevation before and after the bathymetry correction for the site in Figure 2.10a. The 1:1 line is represented by the solid black line.

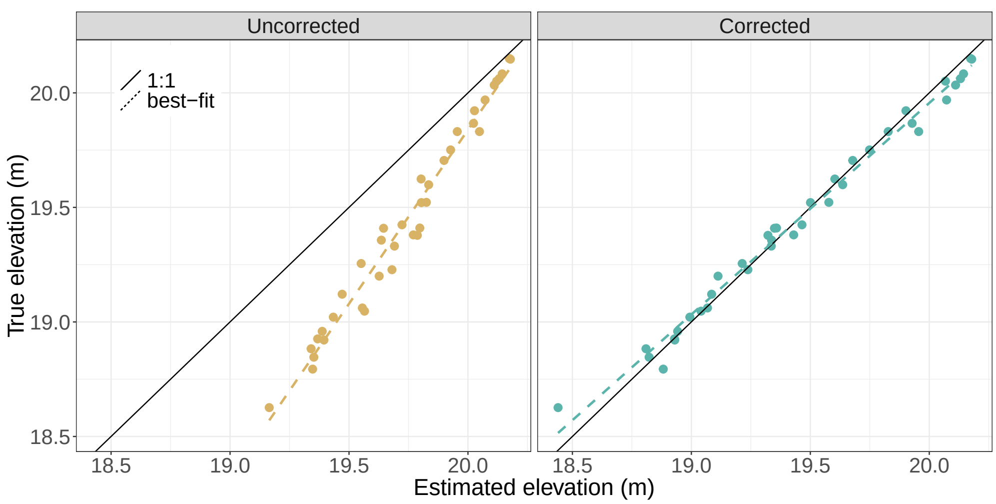

Figure 2.12: Comparison of the submerged bed elevations to the total station measured elevation before and after the bathymetry correction for the site in Figure 2.10b. The 1:1 line is represented by the solid black line.

2.3.2 Survey coverage

The area of channel covered by the RPA and total station in the eight geomorphology study sections were compared to evaluate the total coverage obtainable from the RPA-survey. The area of the channel covered compared to the study section boundaries is illustrated in Figures 2.13 and 2.14, and in Table 2.4. When including side channels in channel boundary, which were generally difficult to access with the RPA due to dense vegetation, it was possible to capture approximately 80% of the bounding area, whereas when only considering the main channel as a boundary, the RPA-survey captured approximately 87% of the bounding area. As time didn't permit all of SA9 to be surveyed with the RPA, the comparison is based on just the lower half of the study section. Figure 2.15 illustrates a situation where dense vegetation and large wood prevented the middle portion of the study section from being captured. Figure 2.16 illustrates how oblique imagery allowed a deep pool covered by overhanging vegetation to be characterized.

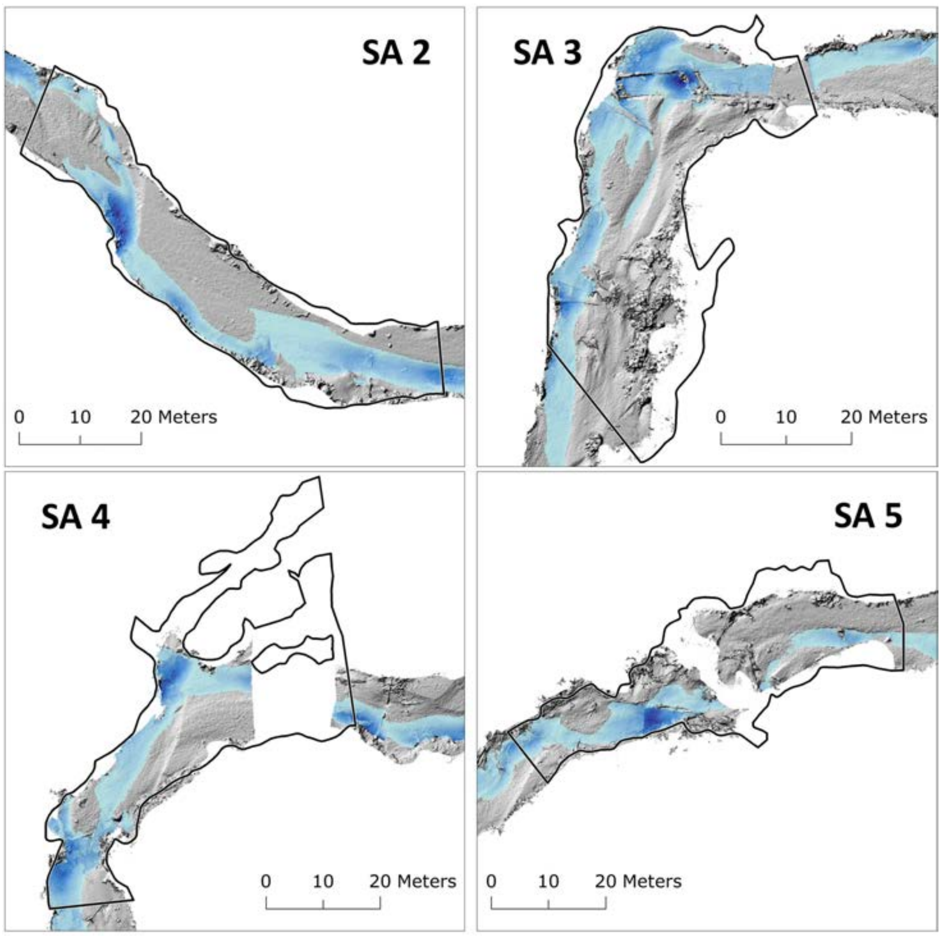

Figure 2.13: RPA coverage overlapped by the study section boundaries indicated in black for SAs 2–5. The texture of the bed surface is displayed through a hillshade layer and the water surface extent in blue, with deeper areas of the channel represented by a darker blue.

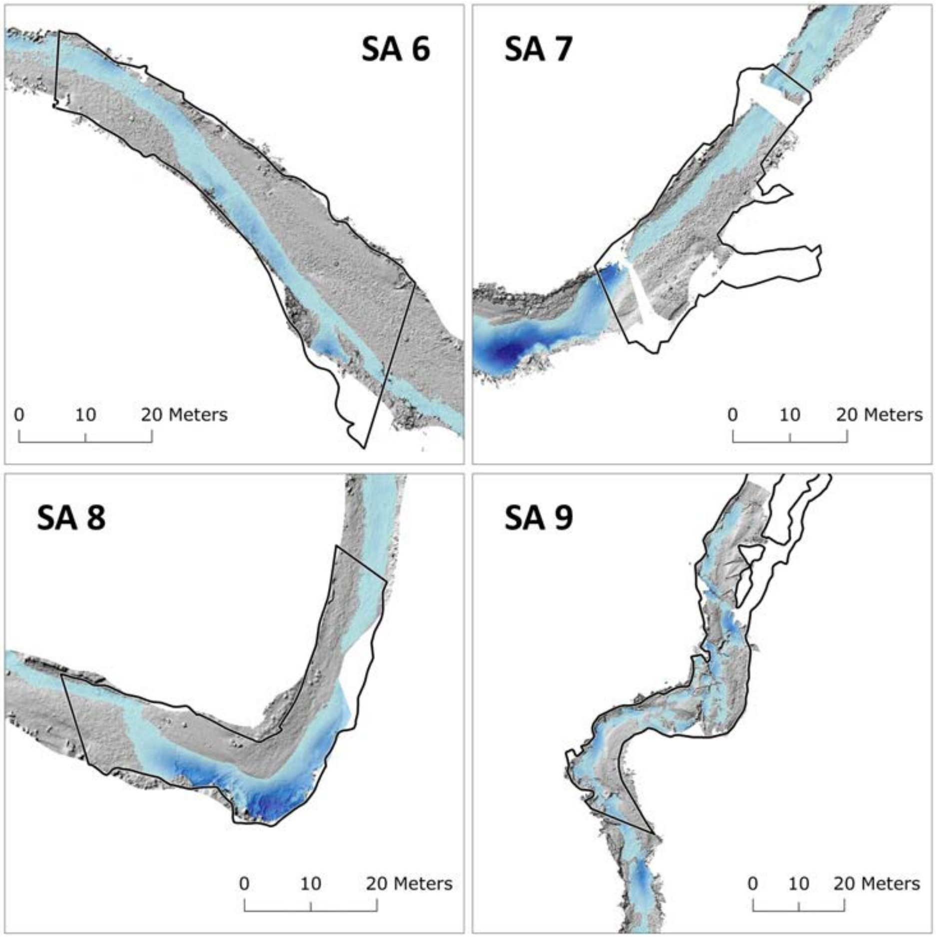

Figure 2.14: RPA coverage overlapped by the study section boundaries indicated in black for SAs 6–9. The texture of the bed surface is displayed through a hillshade layer and the water surface extent in blue, with deeper areas of the channel represented by a darker blue.

Table 2.4: Percentages of the study section covered with the RPA relative to the total station surveys. The comparisons are based on whether the reference boundary included side channels (with side) or just the main channel (no side).

Study section	RPA: with side (%)	RPA:no side (%)
SA 2	90	90
SA 3	83	83
SA 4	54	74
SA 5	81	84
SA 6	91	91
SA 7	67	79
SA 8	94	94
SA 9	89	99
Average	**81**	**87**

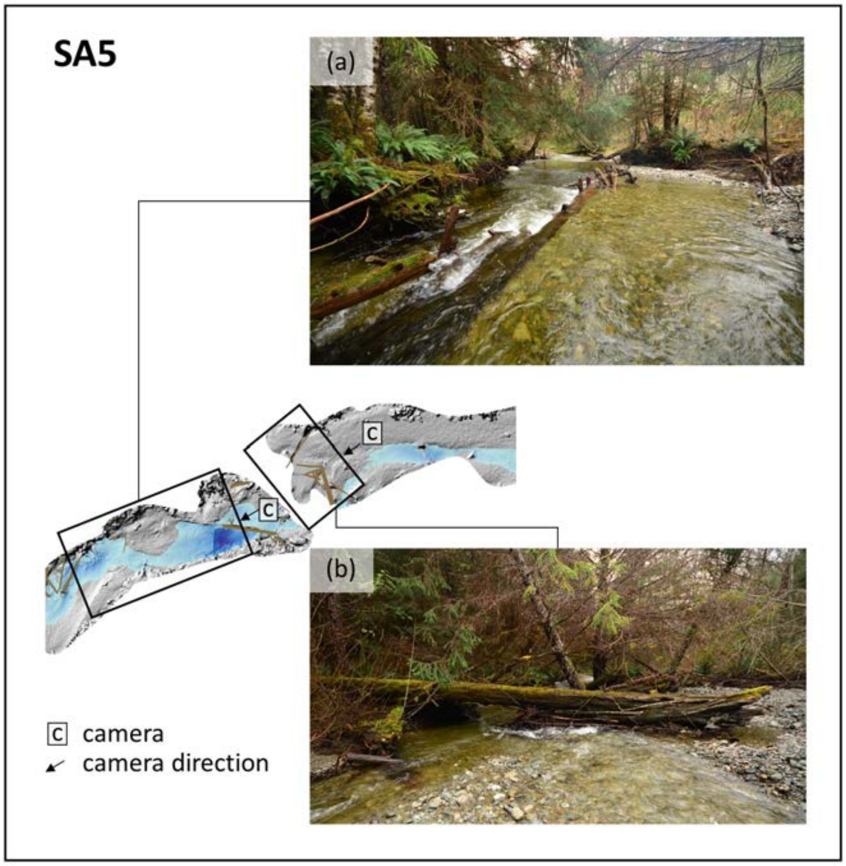

Figure 2.15: Coverage of study section five in an area with low canopy (a) and a missed portion due to dense vegetation and a small log jam (b).The channel's sediment texture is characterized by a hillshade layer and the water extent in blue, with deeper areas corresponding with darker blues. Note that the photo was taken in the fall when the water level was higher than that during the RPA-survey. Photo courtesy of Iain Reid.

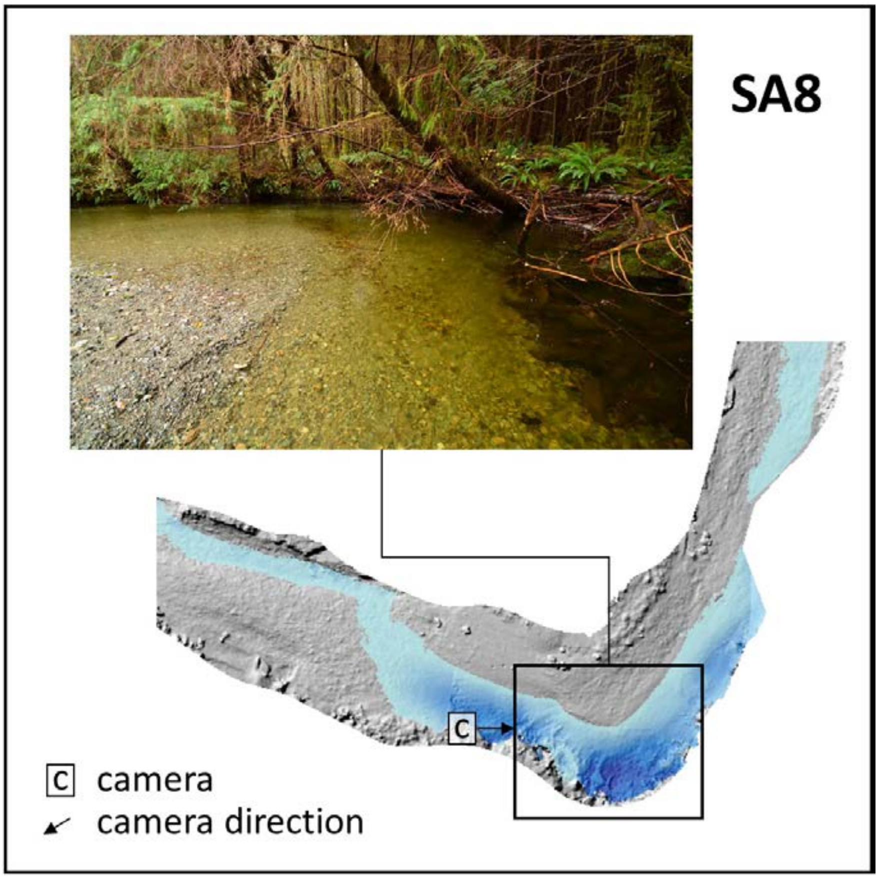

Figure 2.16: Coverage of a deep pool in study section eight under dense riparian vegetation. The channels sediment texture is characterized by a hillshade layer and the waters extent in blue, with deeper areas corresponding with darker blues. Note that the photo was taken in the fall when the water level was higher than it was during the RPA-survey. Photo courtesy of Iain Reid.

2.4 Discussion

The results of this study provide a precedent for using RPAs to characterize channel morphology in small, forested streams using sub-canopy imagery. In twelve field days, three kilometers of channel were surveyed with an estimated coverage rate of 80%. The DEMs and orthophotos created from these images were extremely high resolution at 2 cm / pixel with a RMSE for the exposed elevations of 0.093 m and 0.1 m for the submerged bed elevations. This magnitude of error is comparable to values observed in other studies, such as *Tamminga et al.* (2015), who reported a RMSE of 0.088 m for exposed portions of the bed and 0.11 m for submerged portions of the bed, and *Flener et al.* (2013), who created a DTM of a stream channel using RPA imagery that yielded a RMSE of 0.088 m as well. In comparison to other airborne remote sensing techniques such as LiDAR, these results are comparable to those found by *Legleiter* (2012), who reported a vertical RMSE of 0.21 m. However, the spacing of LiDAR datasets is often on the decimeter scale (*Notebaert et al.*, 2009; *Legleiter*, 2012; *Abalharth et al.*, 2015), which may not be suitable for resolving the sediment texture of the bed in the same manner as has been demonstrated in RPA-surveys (e.g. *Woodget et al.*, 2017). Furthermore, in comparison to LiDAR, RPA imagery offers an affordable and often more accessible tool for characterizing these systems, especially when trying to characterize the submerged bed, which requires the use of expensive green band LiDAR (*Muste et al.*, 2012).

From this high resolution imagery, we demonstrated the utility of methodologies developed by *Woodget et al.* (2017) and *Dietrich* (2017) for accurately extracting sediment texture and bathymetry across the channel in a small, forested stream system. The RMSE values for the submerged bed elevations are comparable to the RMSE values of the field studies conducted by *Dietrich* (2017), who reported RMSE values ranging from 0.06–0.077 m for different surveys of his study site. Using the roughness of the point cloud to derive estimates of grain size across the channel, a strong predictive relationship was acquired for the D_{50} with an r^2 value of 0.92. This is comparable to the r^2 values reported in other studies relating image texture or roughness to predicted grain size (see *Carbonneau et al.*, 2004; *Tamminga et al.*, 2015; *Woodget et al.*, 2017).

The nature of small, forested streams, with their dense canopies, has long left the impression that these characteristics preclude them from the benefits that larger streams have experienced with RPA-surveys. However, through the incorporation of oblique-convergent imagery these results demonstrate that sub-canopy flying of RPAs can provide reasonable coverage of these systems at large spatial extents, as illustrated in Figure 2.8. This application has several advantages over techniques traditionally used to characterize small, forested streams. Pole-mounted photogrammetry, where a camera is attached to a pole suspended several meters above the bed to collect imagery of a site (e.g. *Bird et al.*, 2010) is perhaps the most similar approach to surveying such streams to date. Using this method, *Bird et al.* (2010), surveyed approximately 200m^2 of the bed using 44 GCPs and 14 images that took 10 minutes to capture in a traditional photogrammetric workflow. This allowed the development of a DEM with a ground resolution of 0.03 m and errors within a range of -0.2 to 0.2 m. In comparison to this technique, RPAs provide a greater capacity to collect a larger number of images, which is required for SFM photogrammetry, in a shorter period of time. For example, the channel segment used in the accuracy assessment (Figure 2.5), was approximately 275 m^2, and included the use of 592 photos which took approximately 20 minutes to capture.

In contrast to a total station topographic survey, the sub-canopy RPA-survey allows the collection of a greater density of bed points that can be post-processed to provide continuous measurements of grain size, water depths, large wood and bed elevations across the channel at resolutions that would be challenging to achieve using a total station survey. It is also worthwhile noting that while the total station survey allows for total coverage of the bed, this is through much lower resolution data. The point clouds for the study sections from the total station tend to vary between 500–1000 points, whereas the dense point clouds from the RPA imagery contain millions of points per a reach.

As with each of the previously listed techniques, there are still drawbacks to sub-canopy RPA-surveys. First, due to fallen trees obstructing flight paths and areas with dense low-lying riparian vegetation completely obstructing view of the bed, there is still about 20% of the channel that was not covered with this technique. Depending on the specific research objective, this missing portion may be negligible given the greater longitudinal distance that can be covered with the RPA. However, if assessment of the entire channel is required, it may be necessary to consider a combined approach, such as inclusion of additional total station measurements along with a spatial interpolation method to characterize portions of the channel not observed with the RPA. For example, in delineating aquatic habitat, undercut banks which are situated along the channel edges may be important to identify as they can provide critical cover for salmonids (*Nelson et al.*, 2015). These portions of the channel could be roughly characterized with a modified total station survey that included coarse dimension measurements of the undercuts. Furthermore, although LiDAR is more expensive, it is better suited to penetrating through to the bed in densely vegetated portions of the channel. While the cloth simulation filter did help to mitigate this limitation for the RPA imagery, it still requires that there be viewing angles present that provide perspectives of partially obstructed portions of the bed. In contrast to more traditional aerial platforms, the RPA provided the opportunity to fly below the canopy and capture portions of the bed that would typically be hidden from view of airplane or satellite platforms. However, a disadvantage of this close range imagery is the greater number of photos required to characterize a site and therefore the greater time required for processing the imagery.

There are certain environmental conditions to which the methods discussed in this chapter may also not be suited. Notably, the techniques for extracting the bathymetry may not be suitable for streams with highly turbid water that prevent observation of the submerged bed. Furthermore, areas that were particularly difficult to survey included sections of the channel with low-lying deciduous branches that spanned the channel, that while not fully obstructing the view of the bed, prevented the passing of the RPA. Therefore, these techniques may be most suited to small channels in relatively mature forests that have a more open understory. Finally, while the field time for collecting the data was markedly reduced compared to a total station survey, this came at the cost of greater time required for processing of the imagery. However, with improvements in processing and greater availability of cloud computing resources, this is an area that may see improvement in the future.

Overall, this research helps to expand the toolkit available to geomorphologists for characterizing small, forested streams. Prior to this work, the use of RPAs was restricted to wider channels or those without dense riparian vegetation. The methods described provided high resolution and continuous measurements of bathymetry, grain size and bed elevations that are typically difficult to acquire in small, forested streams. If the corresponding salmonid data were available at the same scale, this spatially continuous dataset would help to bridge the gap between the conceptual theories of the Riverscape Approach proposed by *Fausch et al.* (2002) and the distribution of salmonids in these systems. For example, through using these data to delineate patterns in aquatic habitat in multiple watersheds with the corresponding fish assemblage and abundance data, it may be possible to assess how patterns in aquatic habitat diversity and connectivity impact fish populations. The demonstrated ability to acquire these data provides a step towards helping to fully realize the influence of basin-scale patterns in aquatic habitat on stream fishes.

2.5 Conclusion

This study provided a first attempt at testing the applicability of a sub-canopy RPA-survey for characterizing channel morphology in a small, forested mountain channel. Through the incorporation of oblique-convergent imagery, it was possible to survey 3 km of Carnation Creek at a coverage rate of approximately 80%. Building on prior work analyzing RPA-derived point clouds, information on channel features such as grain size and bathymetry were extracted at resolutions that would be difficult to acquire using traditional survey methods like a total station topographic survey. A drawback to this survey is the significant computation power required to process the data. However, with recent technological advances in cloud processing and photogrammetry software, this is an area that is likely to continue to improve and help make the use of RPA-surveys accessible to the general public. Overall, the methods were very successful in demonstrating the use of RPAs for characterizing small streams with clear water and a relatively open sub-canopy. In contrast to other remote sensing technologies, the RPA-survey described provides a less costly and readily deployable alternative. In particular, this research provides precedent and will hopefully initiate discussion on the role that RPAs can have in characterizing sub-canopy stream systems.

Chapter 3

Rapid and objective classification of channel morphology and diversity at the basin-scale

3.1 Introduction

Advances in the understanding of the relationship between the life processes of some aquatic species and their use of aquatic habitat demand a new approach to aquatic habitat mapping that can be conducted at the basin-scale. This need is well noted by several papers in the 1990s that encouraged characterizing ecological processes in stream systems continuously at a scale relevant to species' life histories, deemed intermediate at 1–100 km in length (e.g. *Schlosser*, 1991; *Fausch et al.*, 2002). When considering the process-based channel morphology classification scheme proposed by *Montgomery and Buffington* (1997), it follows that at these scales streams may display unique characteristics, depending on the arrangement of different morphologies and their driving processes. However, this presents a mismatch with the scale generally used to study aquatic species. Traditional survey techniques are time-consuming and tend to be conducted in study reaches 30–50 channel widths in length. This scale may not be well-suited to characterizing heterogeneity in stream systems, and different approaches to broad-scale mapping of aquatic habitat are needed.

In response to this need, there has been a recent proliferation of studies providing new methodologies to characterize aquatic habitat at these large scales. For example, *Lindenschmidt and Long* (2013) developed a GIS and principal component analysis (PCA) approach to extract channel variables (sinuosity, fractal dimension, width and slope) from coarse DEMs of large streams to identify areas with unique geomorphic characteristics. Several studies have since employed this approach to relate patterns in channel morphologies to patterns in aquatic species assemblages (e.g. *Meissner et al.*, 2016; *Liu et al.*, 2017). However, to date these variables have only been extracted at large scales, with sample sites located as far as every 50 m along the longitudinal profile. While this may help to pull out broad basin-scale patterns, this method is likely to miss heterogeneities across smaller streams that may have an important effect on aquatic habitat. Furthermore, the model was developed for the Little Saskatchewan River, Manitoba, an environment that is different from the small, forested mountain channels common in the Pacific Northwest.

Similar to the work by *Lindenschmidt and Long* (2013), *Hugue et al.* (2016), developed a technique to classify patterns in fast water and slow water channel morphologies across a stream using a PCA. To do this, they used satellite imagery of a 17 km reach from which they derived bathymetry data with 0.5 m resolution in the panchromatic and 2 m in the multispectral. Application of a PCA to the wetted variables derived from a 2D hydrodynamic model allowed them to identify channel types and characterize diversity across the channel based on patterns in velocities and water depths. The meso-scale variables of the analysis provided a good framework suited to identifying local heterogeneities across the channel.

An area that has not yet benefited from rapid characterization of channel morphology using remotely sensed data, as demonstrated by *Lindenschmidt and Long* (2013) and *Hugue et al.* (2016), is small, forested mountain channels. This research seeks to provide a framework for characterizing basin-scale patterns in aquatic habitat of small, forested stream systems that does not require a hydraulic analysis and is rather based on easily extractable metrics from RPA imagery. To build this framework, the chapter aims to meet three objectives:

- Develop a rapid and objective means of characterizing channel morphology near-continuously across the channel (at 1 m intervals) using a PCA-clustering technique on easily extractable RPA data.
- Build upon metrics for characterizing diversity to investigate patterns in channel morphology diversity.
- Investigate the necessary scale required to study the system to ensure that its heterogeneity is captured.

A better understanding of the patterns in channel morphology and diversity is of importance as it is likely to facilitate improved conservation monitoring of these systems.

3.2 Methods

3.2.1 Selection of channel variables

To classify the channel along the longitudinal profile, it was necessary to define a standardized location along which observations would be extracted across the channel. The thalweg was chosen for this purpose as it is a feature that could be easily identified across the channel and would likely highlight patterns key to discriminating channel types, such as differences in slope and water depth. To characterize patterns in channel morphology, five variables were chosen for the classification: the hydraulic radius (R_h), local bed (S_l) and water surface slope (S_{ws}), reach bed slope (S_r), as well as the average D_{50} for cross sections along the thalweg. These channel characteristics reflect larger basin-scale controls on channel morphology, such as geology, climate and land-use that influence watershed conditions (e.g. streamflow and sediment supply) which ultimately give rise to patterns in grain size, channel geometry, bed slope and bed forms across the riverscape (*Buffington and Woodsmith*, 2003). The interplay of these channel characteristics gives rise to unique channel morphologies, and it therefore follows that their extraction should aid in the classification of channel types.

Incorporation of slope

Bed slope was included in the classification, as it helps inform the distribution of channel morphologies across the basin. Channel morphologies tend to progress from pool-riffle, plane-bed, and step-pool to cascade morphologies with increasing channel slope (*Montgomery and Buffington*, 1997). Of this sequence of morphologies, it is the pool-riffle unit that has characteristics that provide both important and functionally different habitats for salmonids (*Hawkins et al.*, 1993). Pools, by nature of their deep and slow moving water, can provide cover and refuge in low flow conditions. In contrast, riffles, which are characterized by fast moving and shallow water, can be an important food source for salmonids via invertebrate drift (*Leung et al.*, 2009; *Naman et al.*, 2018). It is generally accepted that glides (low velocity, depth and slope) and runs (moderate velocity, depth and slope) represent transitional morphologies between these two end members in channel morphology within the pool-riffle unit (*Wyrick et al.*, 2014). It is in these transitional environments, between the tail end of pools and beginning of riffles, that fish tend to spawn, where differences in bed topography lead to hyporheic exchange (*Tonina and Buffington*, 2009), that promote the necessary well-oxygenated conditions for spawning habitat (*Pfeiffer and Finnegan*, 2017). Collectively, the unique characteristics of each of these channel types within the pool-riffle unit provide salmonids with an array of mesohabitats suited to their life histories. Therefore, the reach

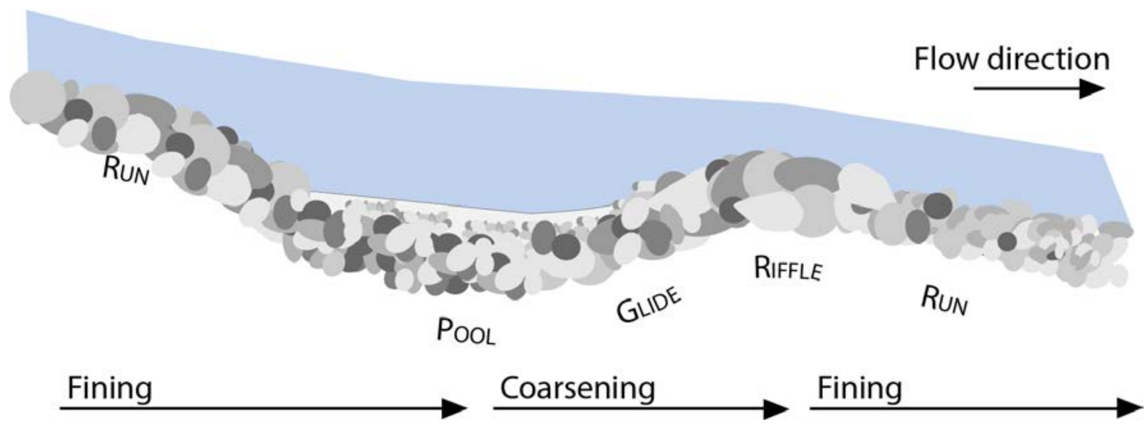

Figure 3.1: Diagram of a typical pool-riffle transition, based on *Garcia et al.* (2012). Note the fining of bed material at the entry of the pool, and coarsening of bed material as the riffle is approached.

scale slope was considered to help aid the discrimination between pool-riffle and plane-bed morphologies closer to the canyon, and the local bed and water surface slope to discriminate between pool, riffle, glide and run morphologies within the pool-riffle unit (Figure 3.1).

Incorporation of hydraulic geometry

The hydraulic radius (R_h) was extracted from the cross sections to provide a measure of the channel's hydraulic geometry. The hydraulic radius was calculated according to Equation 3.1, where A is wetted area and P is the wetted perimeter for the cross section. Essentially, the hydraulic radius indicates how much of the area of water in a cross section is in contact with the bed, with a larger hydraulic radius corresponding with portions of the channel that have less friction imposed on the water and therefore the potential for greater flow velocities.

$$R_h = \frac{A}{P} \tag{3.1}$$

Incorporation of channel roughness

To provide a measure of the grain roughness across the channel, the average D_{50} of the dry exposed bars in a 0.5 m buffer around each cross section was extracted. According to the Lane Balance (3.2) (*Lane*, 1955), in an equilibrium channel, grain size reflects a balance between channel conditions, such as slope (S), discharge (Q) and sediment flux (Q_s). The interplay of these governing conditions determines channel morphology (*Church M.*, 2002). Indeed, there is a general coarsening in bed material from glides and pools with finer material to riffles and runs (*Garcia et al.*, 2012).

$$D \;\alpha\; \frac{QS}{Q_s} \tag{3.2}$$

3.2.2 Extraction of channel variables

Thalweg extraction

To extract the thalweg, the River Bathymetry Toolkit (RBT), an ArcMap add-in, was applied to the RPA-derived DEMs generated of the bed across Carnation Creek (*McKean et al.*, 2009). Inputs for the thalweg tool of the RBT include a detrended DEM, bankfull polygon and channel centreline. The tool expects a DEM that approximates the valley and channel bed, as opposed to roughness elements such as large wood, which the RPA imagery does not provide. To mitigate this, a pseudo-valley was established by fitting a plane through the point clouds of the channel bed and adding 1.5 m to the planes to approximate the channel valley. Channel obstructions such as large wood were also clipped from the point clouds in Cloud Compare and their bed elevations interpolated using inverse distance weighting to create clean and complete DEMs of the channel bed. The cleaned DEMs were then merged with the valley planes and the 'detrend' tool in the RBT applied to them.

To provide estimates of the channel centreline, the 'collapse dual lines to centreline' tool was applied to polylines of the right and left bank in ArcMap. With the detrended DEM, bankfull polygon and centreline as inputs, the thalweg was extracted using the 'thalweg' tool of the RBT. The tool runs a least-cost-path analysis based on the centreline and channel elevations, with deeper sections of the channel receiving a higher weighting to determine the thalweg.

Feature extraction along thalweg

To characterize patterns in channel morphology along the thalweg, a function was developed to sample points along the thalweg every metre at which the hydraulic radius (R_h), local bed (S_l) and water surface slope (S_{ws}), reach bed slope (S_r), as well as the average D_{50} for a neighbourhood were extracted from the RPA derived rasters of the bed elevations, bathymetry and D_{50} as described below and illustrated in Figure 3.2. Cross sections where the channel banks were not discernable (e.g. due to channel obstructions or dense low-lying vegetation) were excluded from the analysis.

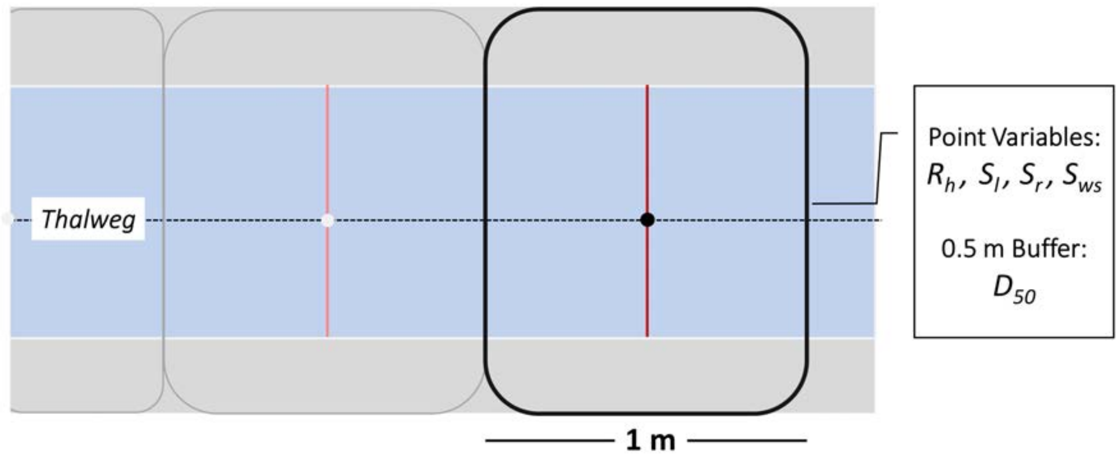

Figure 3.2: Feature extraction set up. The R_h, S_l, S_{ws}, and S_r were extracted every metre. The average grain size was extracted every meter based on the average value of the D_{50} raster in a 0.5 m buffer around each cross-section line.

Slope extraction

The local slopes of the bed and water surface were calculated for each sampling location using a function in R that fits a linear model through observations in a 15-metre window around each sample site. This window size was chosen based on field observations at Carnation Creek that suggested it would be sufficient for capturing smaller scale patterns in slope within the pool-riffle unit. This was repeated for the reach-scale bed slope using a 45-metre window based on previous knowledge that this is equal to the average pool-riffle spacing at Carnation Creek (S. Bird, personal communications, April 2018).

Hydraulic radius extraction

In wide and shallow channels, the hydraulic radius can be well approximated by the water depth. However, many of the pools along Carnation Creek occur in deep and narrow sections of the channel, thus violating the wide channel approximation assumption. Therefore, the hydraulic radius for all cross sections across the channel was calculated using Equation 3.1. To calculate the length of the wetted perimeter, the wetted cross section lines were first converted to 3D polylines in ArcMap using the 'Interpolate Shape' tool from the 3D Analyst Toolbox. This attributes depths to the cross section lines every 10 cm from the bathymetry rasters. The wetted perimeter of each cross section was determined by using the 'Add Surface

Information' tool in ArcMap from the 3D Analyst Toolbox. For each wetted perimeter line, the area below a plot of distance along cross section against water depth was then calculated using the 'trapz' function in the Practical Numerical Math Function ('pracma') package in R (*Borchers*, 2018). The hydraulic radius was then calculated as the wetted area at each cross section divided by its wetted surface length.

D_{50} extraction

To provide a measure of the grain roughness across the channel, the average D_{50} of the dry exposed bars in a 0.5 m buffer around each cross section was extracted. Together, these variables summarize the channel form (R_h and S) and roughness (n, approximated by D_{50}) of each cross section, akin to the variables used for the Manning Equation (1891) (Equation 3.3), which provides an estimate of the channel's velocity. Therefore, there is mathematical impetus to using these variables to discriminate between slow-moving residual pools and faster riffle morphologies that will provide unique aquatic habitats.

$$v = \frac{1}{n} R_h^{\frac{2}{3}} S^{\frac{1}{5}} \tag{3.3}$$

3.2.3 Principal component analysis

Using the extracted channel variables, an attempt was made to rapidly and objectively characterize channel morphologies using a PCA and k-means clustering algorithm using the package 'stats' in R (*R Core Team*, 2018). The general purpose of a PCA is to reduce the number of dimensions in a dataset that contains interrelated variables while describing the maximum amount of variation present (*Jolliffe*, 2002). This is achieved by a transformation that projects the data along principal components, which are axes that best explain the variation of the data, with the first component explaining the most variation, followed by the remaining components (*Jolliffe*, 2002). Throughout the transformation, the relative positions of the observations to one another remain the same. This allows components which do not explain much of the variation to be removed, thereby allowing the data to be visualized using fewer dimensions. Because the dataset was multi-dimensional, with five variables over 2362 sampling sites, a PCA was an appropriate analysis tool to help simplify and pull out patterns in the data, which is beneficial for k-means clustering.

Eigenvector selection

The PCA was first run using all five dimensions, from which a decision was made on how many dimensions were necessary to explain the variation in the data. To make this decision, the cumulative percentage of variation explained by the principal components, as well as the variation explained by each eigenvector was examined. Eigenvectors are vectors that explain the directions along which the data varies, whereas eigenvalues explain the amount of variation explained by each of the principal components. A commonly used rule to determine the number of components to use is to choose a cut-off value between 70% and 90% for the cumulative variance explained by the components (*Jolliffe*, 2002). The scree plot in Figure 3.3 shows that the first two and first three components explain 64.6% and 79.0% of the variation in the dataset, respectively. This suggests that three components would be a suitable number to retain. Considering the eigenvalues of the principal components (Figure 3.4) shows that the first two components have eigenvalues greater than or close to one. An eigenvalue of less than one represents components which explain less variance than one of the original variables (*Jolliffe*, 2002). However, to allow for sampling variation, it has been suggested that an eigenvalue cut-off value of 0.7 may be appropriate (*Jolliffe*, 2002). As the third component has an eigenvalue of 0.73, an argument can be further made for retaining just the first three principal components.

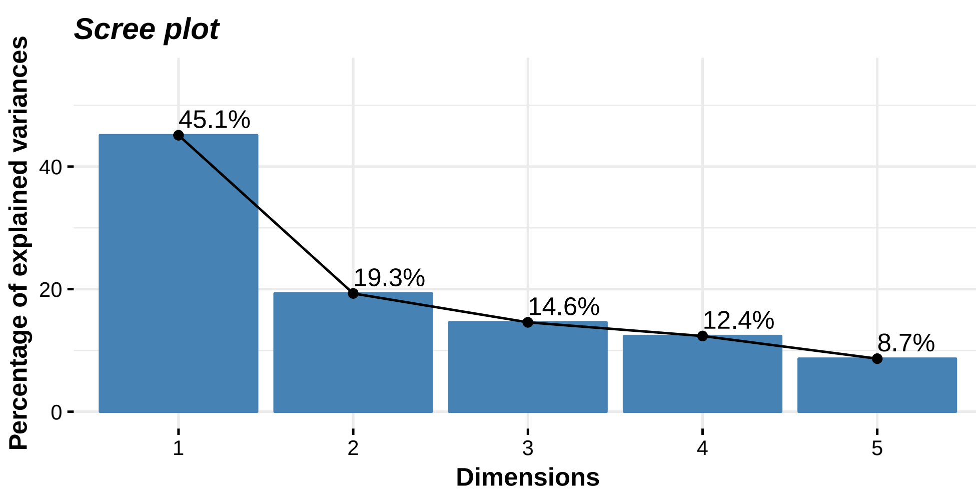

Figure 3.3: Scree plot of the variance explained by the principal components.

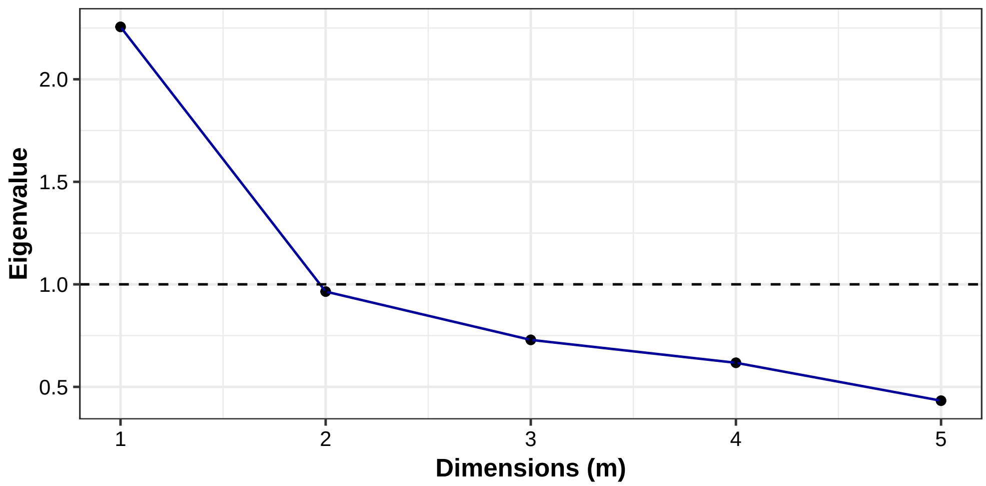

Figure 3.4: Eigenvalues representing variance explained by the principal components (dimensions).

3.2.4 K-means clustering

Following the PCA, a k-means clustering algorithm was run to identify clusters in the data along the first three components. A k-means clustering algorithm is an unsupervised classification that assigns observations from 'n' dimensions to clusters that allow the within-cluster sum of squares to be minimized (*Hartigan and Wong*, 1979). A key decision in a clustering analysis is determining the number of clusters to be used to classify the data. Initially when adding more clusters, the variation within each group will steeply decrease, but eventually there will be a point where the addition of more clusters has a marginal influence on decreasing the within-cluster variance. This point, which would be located at an elbow or plateau in a plot of clusters against within-cluster variance is often deemed an appropriate point to choose as a cut-off (*Flynt and Dean*, 2016). To identify this location, the k-means clustering algorithm was run with the number of clusters ranging from one to 20 (a value greater than the number of morphologies to be expected at Carnation Creek) and a plot of within-cluster variance against number of clusters examined. As seen in Figure 3.5, at about 5–7 clusters the curve becomes much less steep, which matches well with the number of morphologies one may expect at Carnation Creek, being pool, riffle, run, glide and plane-bed morphologies near the canyon. Therefore, the k-means clustering algorithm was run with the number of clusters set to six.

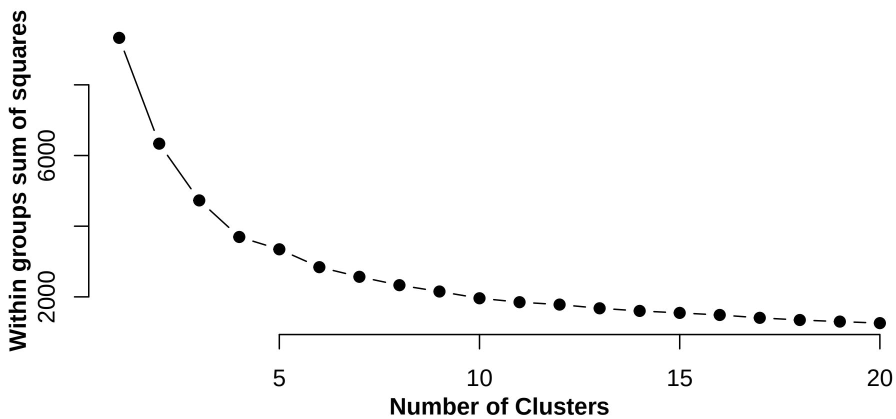

Figure 3.5: K-means clustering plot demonstrating how the within groups sum of squares decreases with the incorporation of more clusters.

3.2.5 Channel diversity classification

Following clustering of the cross-sectional variables, the mean values for each of the channel variables of each cluster were examined and a channel type was attributed to each cluster. This provided a continuous classification of channel types across Carnation Creek from the mouth to the beginning of the canyon at 1 m intervals. From these data, a measure of channel diversity was acquired throughout the stream. To characterize the diversity of channel morphology across the stream, a moving analysis using the Shannon diversity index (*Shannon and Weaver*, 1964) was conducted. The Shannon diversity index provides a measure of the abundance and evenness in an area (*Lloyd and Ghelardi*, 1964). Whereas it is often calculated with regard to species types in ecology, in the context of this research channel types are instead considered, similar to the work of *Harris et al.* (2009). To calculate it, the proportion of each channel type (p_i) in an area is multiplied by the natural logarithm of the proportion. This value for all the channel types present in the system is summed up yielding the Shannon diversity index (Equation 3.4).

$$H = -\sum p_i ln p_i \tag{3.4}$$

3.2.6 Scale effects

Finally, a relevant question with regards to managing these systems is determining the scale that needs to be surveyed to ensure that their heterogeneity is likely captured. To answer this, the standard deviation of diversity was calculated for window sizes ranging from 15–600 m in length. It would be expected that eventually the standard deviation would approach a finite value with increasing sample size, providing an estimate of how much of the channel it is necessary to survey to ensure that its heterogeneity is captured.

3.3 Results

Interpretation of the PCA

The first three components from the PCA explained approximately 80% of the variation in the data, with components one, two and three reflecting 45.11%, 19.3% and 14.6% of the variation respectively. The contributions of each variable to each component are illustrated in Figure 3.6, with larger contributions indicating that the variable has a greater influence on the component. The first component is most largely represented by S_r, D_{50} and S_{ws} (Figure 3.6a), the second by the R_h (Figure 3.6b), and the third by the S_l and D_{50} (Figure 3.6c).

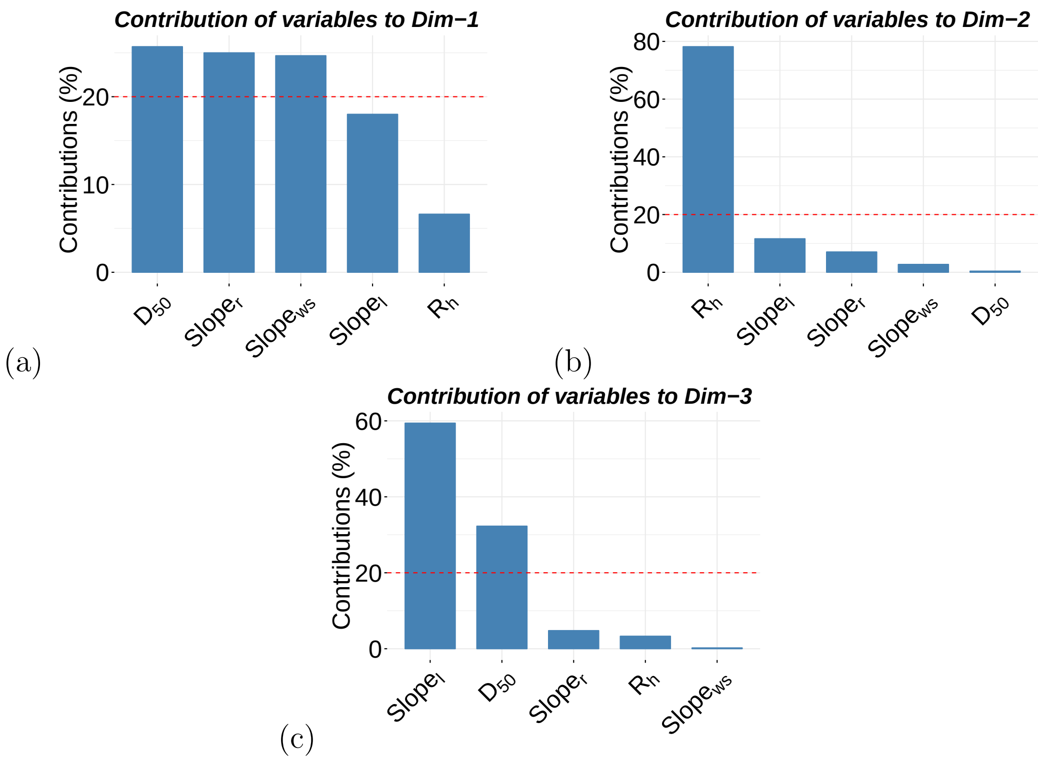

Figure 3.6: Variable contributions to Principal Components. The red-dashed line represents the mean contribution of the variables at 20%.

The correlation circle, Figure 3.7, provides a representation of the quality and correlation of the variables with one another along the first two components. Variables that are of high quality along a dimension are represented by their high cos2 value and the greater distance they plot from the circle's centre. Variables that are closely related tend to plot close to one another, while those that are inversely related tend to plot at 180° from one another, and those with no relation tend to plot perpendicular to one another. As seen in Figure 3.7, D_{50}, S_r and S_{ws} are of relatively high quality and plot in a slightly opposite direction to the R_h. S_l is of relatively low quality, but plots in the same direction as D_{50}, S_r and S_{ws}, suggesting that the variables are weakly correlated.

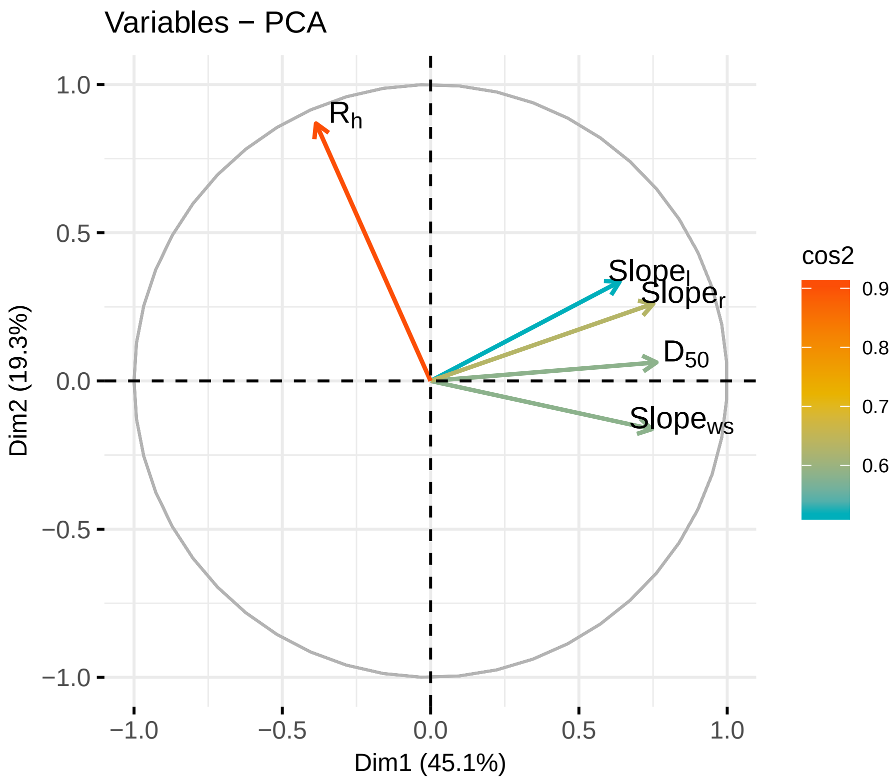

Figure 3.7: Correlation circle plot. The colour ramp describes the quality of the representation along the component.

3.3.1 Clustering analysis

After running the k-means clustering algorithm using six groupings on the first three components, similar patterns appear in the biplot (Figure 3.8 and Figure 3.9), compared to those observed in the correlation circle (Figure 3.7). For each cluster, the mean of each variable was determined and the likely morphology attributed to it based on these values (Table 3.1). Moving from left to right along the first dimension there is a transition from morphologies with shallow bed and water surface slopes with finer material, to steeper morphologies with coarser material (Figure 3.8). This appears to represent a transition from pool to riffle morphologies along the first component. Within the riffle channel type, the classification also captures a distinction between riffle morphologies with slightly coarser bed material, which received the channel type "Riffle-coarse" (Riffle$_C$) to characterize this change. Moving down the y-axis, shallower environments are encountered with decreasing local bed slopes, as indicated by the transition from pool to glide morphologies (Figure 3.8).

Table 3.1: Means of channel variables for each cluster. l is the longitudinal distance, d is the thalweg depth, R_h is the hydraulic radius, S_l is the local slope, S_{ws} is the water surface slope, S_r is the reach slope, D_{50} is the median grain size and W is the channel width.

Cluster	l (m)	d (m)	R_h (m/m)	S_l (m/m)	S_{ws} (m/m)	S_r (m/m)	D_{50} (cm)	W (m)
Riffle$_C$	2980	0.16	0.12	0.018	0.018	0.024	6.74	4.13
Plane-bed	3160	0.20	0.14	0.054	0.047	0.042	8.21	3.47
Riffle	1650	0.13	0.090	0.027	0.016	0.012	4.10	3.65
Glide	1470	0.28	0.16	-0.020	0.003	0.003	3.68	4.99
Run	1435	0.61	0.35	0.044	0.005	0.016	3.92	4.94
Pool	1420	1.04	0.60	-0.031	-0.004	0.000	3.66	5.99

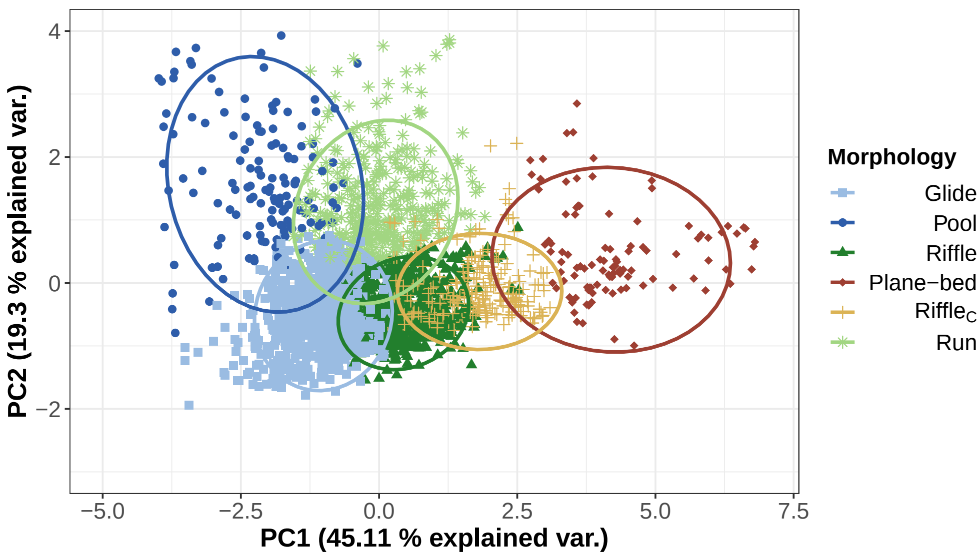

Figure 3.8: Biplot of each observation along PC1 and PC2. The groupings from the k-means clustering analysis are colour-coded and their centroid outlined.

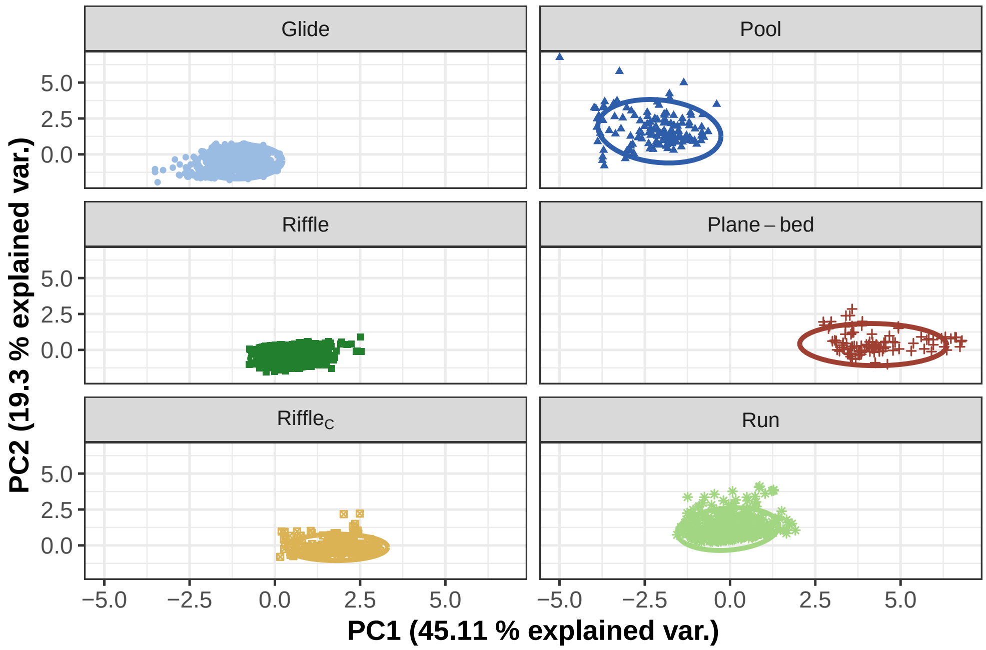

Figure 3.9: Isolated biplot of each observation along PC1 and PC2 for the six clusters. The groupings from the k-means clustering analysis are colour-coded and their centroid outlined.

3.3.2 Clustering accuracy assessment

To assess the accuracy of the clustering algorithm, 100 locations were randomly selected along the thalweg and visually assigned to either glide, pool, run, riffle, riffle$_C$, or plane-bed morphologies according to Figure 3.1. These values were then compared to the morphologies predicted by the PCA. As seen in Table 3.2, there was 85% agreement between the PCA classified morphologies and visually classified morphologies. The riffle morphologies had the lowest correct classification rate at 71.8% and 77.0% for the riffle and riffle$_C$ categories, respectively. Glide and plane-bed morphologies had the highest classification rate at 97.4% and 100%, respectively.

Table 3.2: Accuracy assessment of morphology classification

Morphology	**% Correct**
Glide	97.4
Pool	80.0
Run	84.6
Riffle	71.9
Riffle$_C$	77.7
Plane-bed	100 .0
All	85.0

The trends of the clustering analysis generally match what is observed in the field. The increase in the plane-bed morphology observed around 3000 m in Figure 3.10 corresponds to what is observed at Carnation Creek (Figure 3.11). When approaching the canyon there is a sudden and marked change in morphology, with the slope becoming steeper (Figure 3.12) and bed material much coarser, which the plane-bed cluster appears to capture. This channel type is characterized by shallower water depths, very steep reach scale slopes (S_r = 0.042 m) and nearly double the average grain size (D_{50} = 8.21 cm) found in lower reaches of the channel.

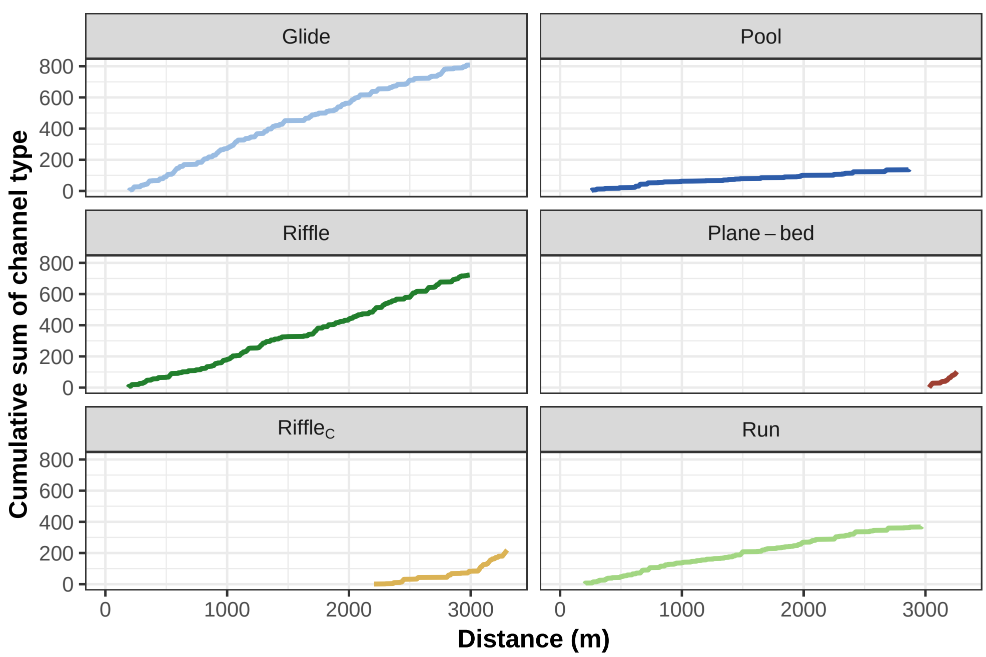

Figure 3.10: Cumulative sum of channel morphologies along the stream's longitudinal profile.

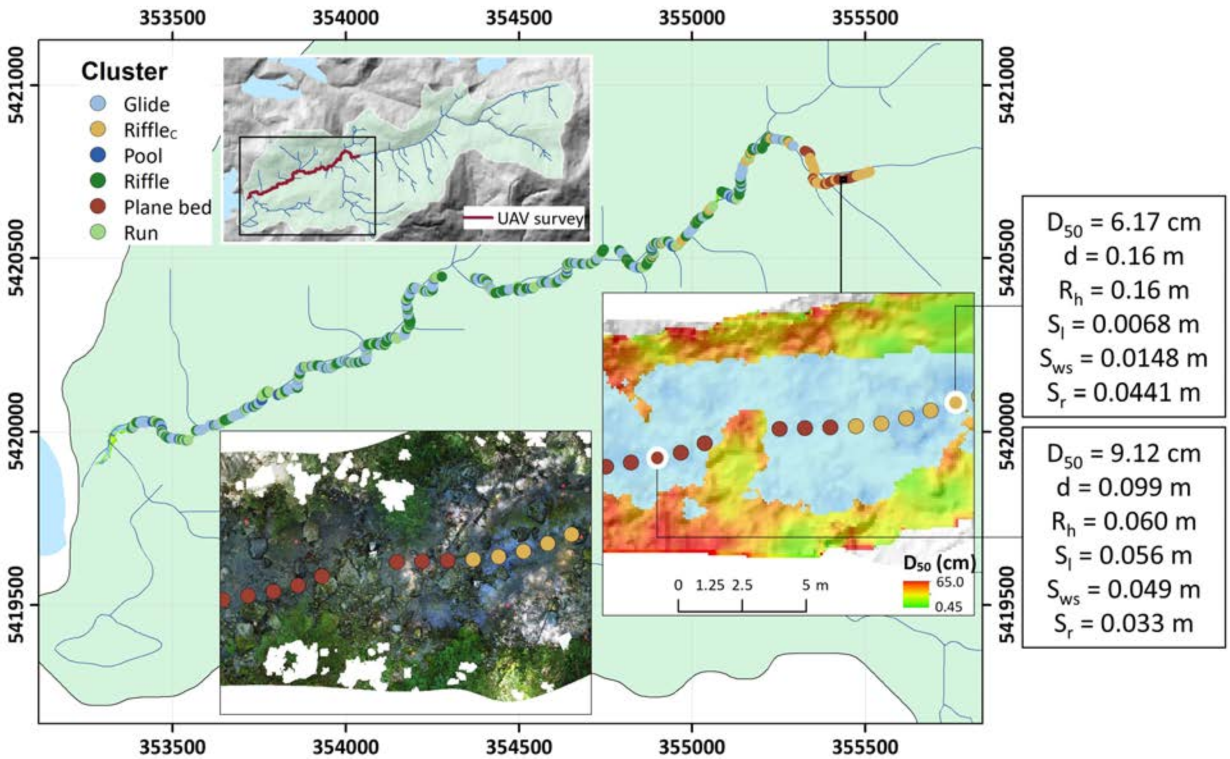

Figure 3.11: Distribution of channel morphologies at Carnation Creek. At ∼3000 m upstream, there is a marked change in channel morphologies from the typical riffle-pool morphologies to much steeper and shallower channel morphologies.

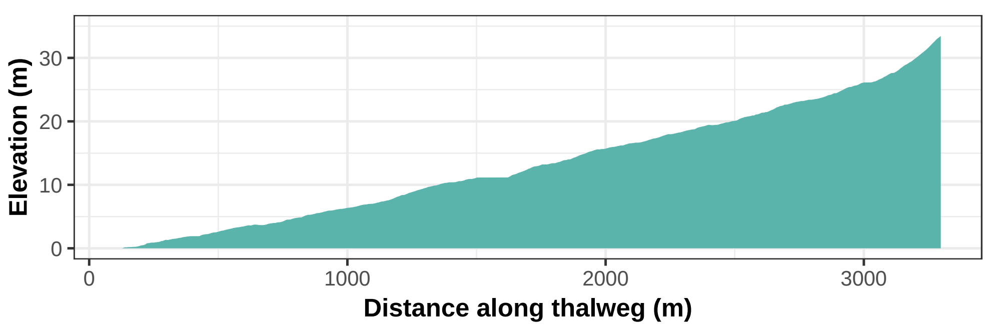

Figure 3.12: Longitudinal profile along the thalweg of Carnation Creek.

In a heterogeneous area further downstream in the channel, the classification matches the typical progression expected of channel morphologies (Figure 3.13) in a pool-riffle transition area. The exit of the pool is classified as a glide, with negative channel slopes. As the slope gets a little steeper we see shallow riffle type morphologies that meld into a deeper run at the entry of the pool (Figure 3.13).

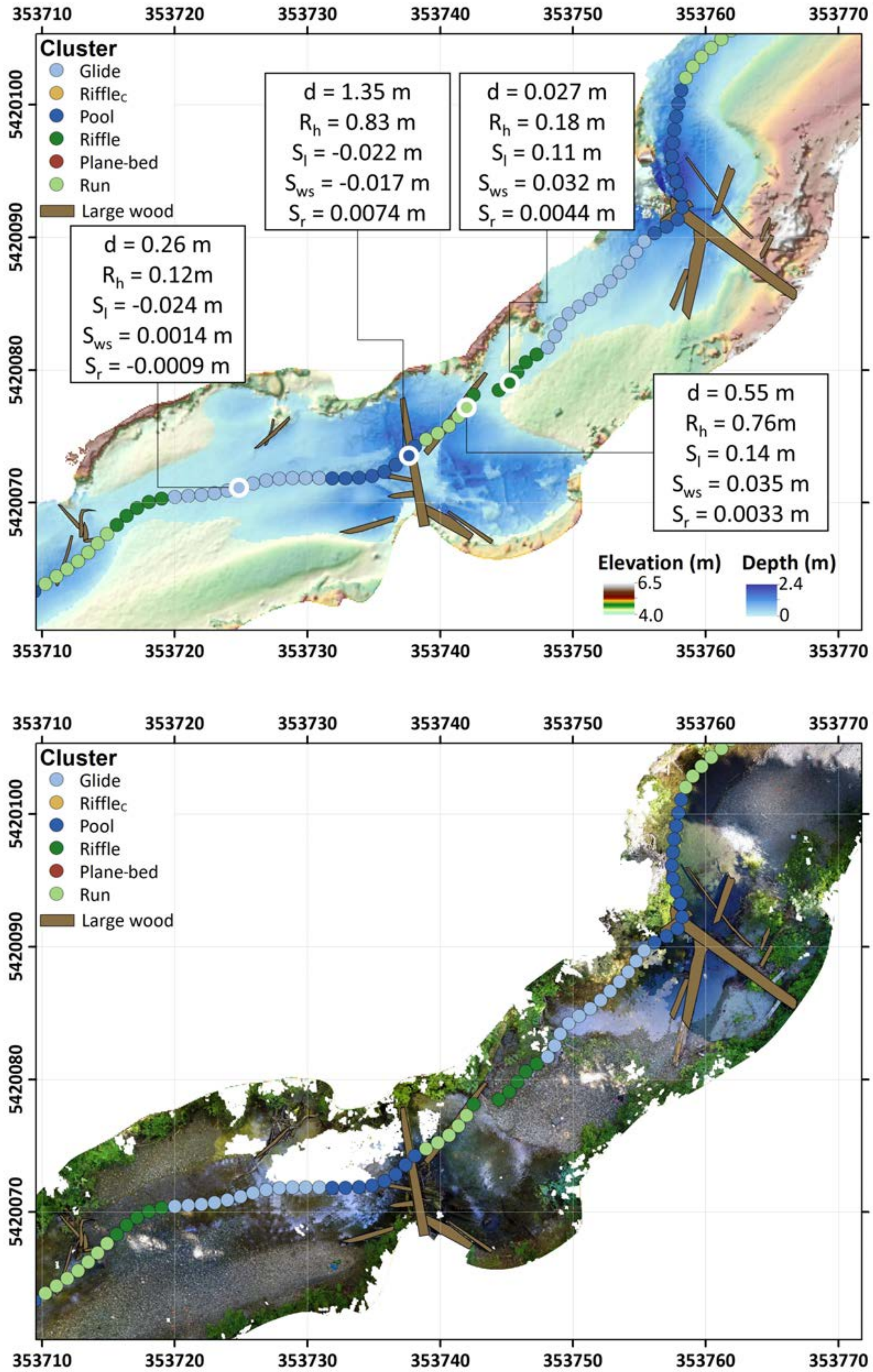

Figure 3.13: The transition of channel morphology from riffles to pools in a heterogeneous section of channel.

The channel morphology classification is also sensitive to changes in bed slope and grain size (Figure 3.14). This is evidenced in study section seven, where there is an initial coarsening in bed material and steepening in bed slope where a tributary enters the channel. Rather than receiving a riffle classification (typical $S_r = 0.012$ m/m and $D_{50} = 3.65$ cm), this unique section of the channel received the riffle$_C$ morphology classification which is characterized by a slightly steeper slope and larger grain sizes (typical $S_r = 0.024$ m/m and $D_{50} = 6.74$ cm). Figure 3.14 demonstrates how the PCA-clustering technique can identify local areas with unique morphological characteristics that may be missed in a traditional view of the system.

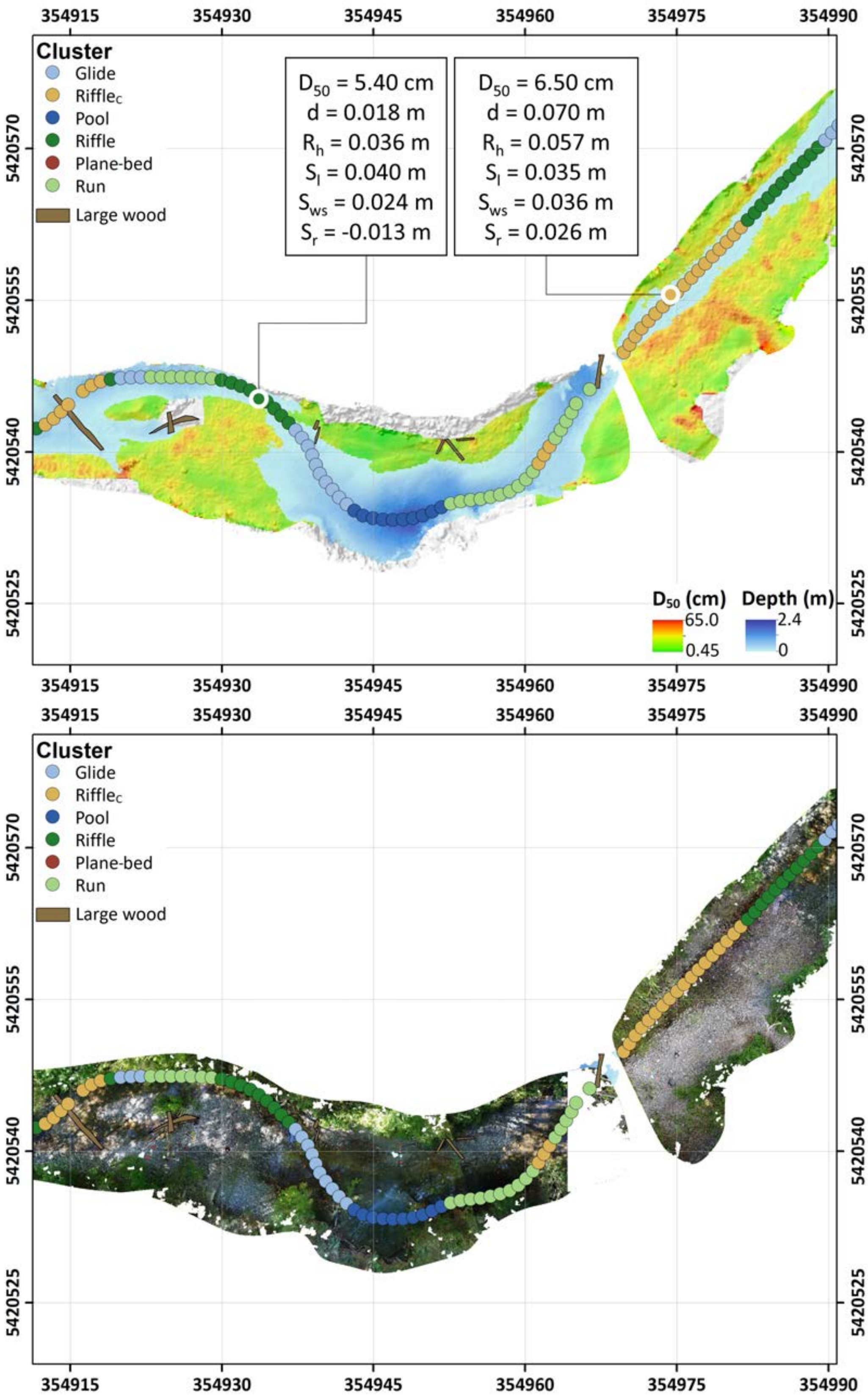

Figure 3.14: The influence of grain size and slope is indicated by the classification of riffle$_C$ morphology in study section seven, where a tributary enters the channel.

3.3.3 Scale effects

Because fish require an array of physical habitats to complete their life histories, it would likely be useful from a management perspective to have a metric that characterizes patterns in channel diversity across the river basin. Such a metric was provided by calculating the Shannon's diversity index of channel morphologies at one-metre intervals in a 45-metre window. As demonstrated in Figure 3.15, diversity fluctuates greatly at the 45-m scale, however, there appears to be a trend towards decreased channel diversity as the canyon is approached.

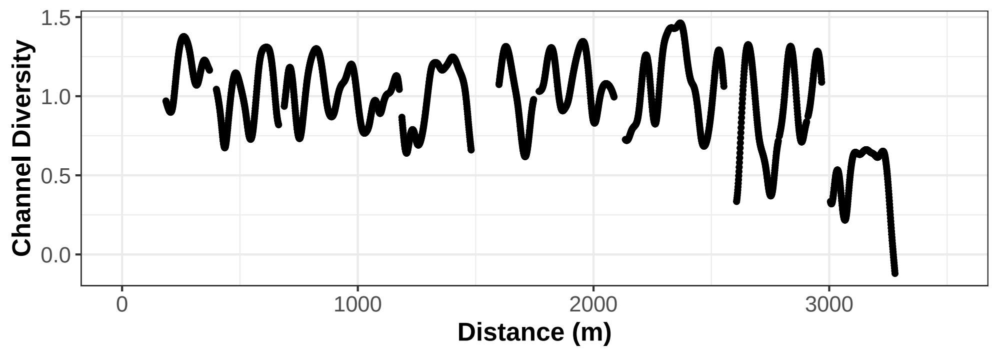

Figure 3.15: Shannon's diversity across the channel based on a 45-metre window. Gaps in the data correspond with locations where there were no survey observations in a window.

Finally, we were interested in assessing how much of the channel it was necessary to survey to ensure that its heterogeneity was captured through analyzing the change in standard deviation of channel diversity for different window sizes. This assessment was limited to the lower three kilometers of the channel, prior to the onset of the plane-bed morphologies, which are not used by anadromous salmon. The results of calculating the standard deviation of the diversity metric for channel types from windows ranging from 15-600 m in length can be observed in Figure 3.16. After a window size of around 200 m in length, there are marginal decreases in the standard deviation of channel diversity with increasing window size. This suggests that at around this distance, it is likely that the diversity of channel types will be captured.

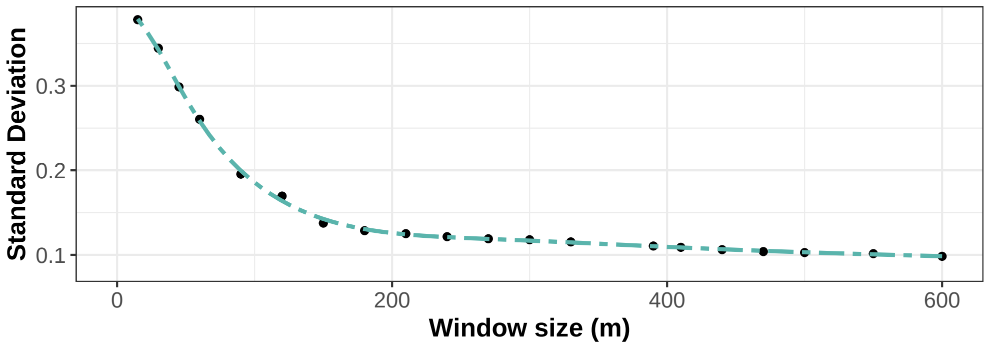

Figure 3.16: Standard deviation of channel diversity.

3.4 Discussion

This study shows how RPA imagery can be used to objectively and rapidly characterize patterns in channel morphology at the basin-scale of a small, forested mountain channel. Using remotely sensed data and a PCA-clustering analysis, three kilometers of channel were characterized along the longitudinal profile at 1 m intervals. This is a resolution and extent traditionally difficult to capture in small, forested channels, yet is of critical importance for the life cycles of some aquatic species (*Fausch et al.*, 2002). In contrast to prior PCA-clustering analysis (*Lindenschmidt and Long*, 2013; *Hugue et al.*, 2016), this research demonstrates how easily extractable RPA-centric variables can be used without running computationally-expensive flow models to classify the channel. Following a k-means clustering algorithm, six unique channel morphologies were identified, with an overall correct classification rate of 85%.

A strength of the PCA is the ability to investigate patterns in the data that influenced the observed classification. As illustrated in Figures 3.6 and 3.7, the general relations between the variables comprising the three components used in the analysis match our geomorphic understanding of stream systems. The first component is well represented by S_{ws}, S_{45} and D_{50}, the second by R_h, and the third by S_l. Therefore, the first component is characterized by variables known to share clear trends along the longitudinal profile (*Buffington and Woodsmith*, 2003), whereas the second and third describe more local conditions, relating to the local channel geometry and slope respectively. As shown in Figure 3.7, S_{ws}, S_{45} and D_{50} are of relatively high quality and plot in a slightly opposite direction to R_h, indicating that these two sets of variables are inversely related. Indeed, one would expect pools, areas that tend to have smaller water surface and reach slopes to have a greater hydraulic radius. As the D_{50} plots near S_{ws}, S_{45}, it is well correlated with reach scale patterns in slope, indicating that steeper portions of the channel are likely linked with coarser grain sizes, as has been noted in the literature (*Buffington and Woodsmith*, 2003). Local channel slope was the lowest quality variable, likely due to the array of channel slopes associated with similar channel geometries in transitional areas. It was most well represented on PC3, which had an eigenvalue of less than one, meaning that it explains less variation than a single variable of the original untransformed dataset (*Jolliffe*, 2002). There could therefore be an argument made for excluding PC3 from the analysis. However, it is the component which had the strongest and highest quality representation of local channel slope (Figure 3.6c), which is likely an important discriminator of meso-scale morphologies such as glides, which tend to have local negative slopes. Therefore, the third component was included in the analysis, to be conservative in ensuring local channel slope was well represented.

Examination of the classification from the PCA-clustering analysis revealed that there was good agreement between the characteristics of the morphologies with those found in previously published studies. As shown in Table 3.3, the mean values of the variables for each assigned morphology are close to reference values found for the slope, depth and grain size characteristics of similar channels. The accuracy of the PCA-clustering technique was also tested against a visual classification of random locations along the channel. The greatest disagreement in the channel morphologies came from the riffle and riffle$_C$ morphologies at classification success rates of 71.9%, and 77.7% respectively. Determining the morphology of transition zones, such as between runs and riffles appeared to be a source of confusion between the classification schemes. In contrast, plane-bed and glide morphologies were easily distinguishable through their unique slopes and grain sizes (Table 3.1), thus leading to their correct classifications. As the visual classification is subjective, it is not surprising the two classification schemes do not have 100% agreement. Ultimately, the PCA-clustering technique presented provides an objective alternative with a statistical basis.

Table 3.3: Comparison of average values for variables of each morphology to those found in previously published studies. X$_{Church}$ refers to values referenced from *Church* (1992), X$_{Hogan}$ to values referenced from *Anonymous* (1996), and X$_{Buff.}$ to values referenced from *Buffington and Woodsmith* (2003), and X$_{Helm}$ to values reported in this research.

Morphology	***S$_{Church}$ (m/m)***	***S$_{Hogan}$ (m/m)***	***S$_{Buff.}$ (m/m)***	***S$_{Helm}$ (m/m)***	***D/d$_{Church}$ (m)***	***D/d$_{Hogan}$ (m)***	***D/d$_{Helm}$ (m)***
Riffle	0.02	0.005-0.015	0.001-0.02	**0.012**	<1.0	0.1-0.3	**0.328**
Riffle$_C$	-	0.015-0.03	-	**0.024**	-	0.3-0.6	**0.411**
Plane-bed	0.02-0.04	0.03-0.05	0.01-0.04	**0.042**	~1	0.6-1.0	**0.419**
Glide	-	-	-	**0.003**	-	-	**0.134**
Run	-	-	-	**0.016**	-	-	**0.064**

A useful contribution of this research for watershed management was formed by the metrics that were developed to characterize the channel's heterogeneity. The application of Shannon's diversity index, a frequently used metric in ecology for investigating the structure of ecosystems, was a new application in the assessment of diversity of channel morphology of a small, forested stream. As demonstrated in Figure 3.15, there was a decrease in diversity with distance upstream, which matches observations in the field. Certainly as the canyon is approached at around 3000 m, there is a decrease in diversity as the channel transitions to plane-bed morphologies. However, overall channel diversity fluctuates greatly at the 45-metre reach scale, further elucidating the importance of considering the Riverscape Approach for studying these systems that may not vary consistently and predictably. In reality though, many long-term research experiments still rely on using discrete reaches to understand watershed processes. Therefore, to provide a useful tool for managers, an estimate was made on the required scale to study Carnation Creek to ensure its heterogeneity was characterized. This was predicted to be approximately 200 m, and intriguingly is close to the sediment storage wavelength identified by (*Reid et al.*, 2019) for the system. This number can provide insights for setting up studies like the one observed in Carnation Creek.

Perhaps the greatest strength of the PCA-clustering technique is its implicit suitability to the study area of interest. Each stream is unique, and therefore it is possible that imposing unit boundaries discovered in one stream will not yield realistic groupings in a new system. Rather, the PCA-clustering technique finds natural groupings in the dataset that may be better suited to the area of interest. The RPA-survey as a means of data collection also provides an improvement over traditional methods. Extraction of channel widths typically is a task that would require at least two people, and care must be taken in the field to properly collect the data at systematic intervals and transcribe the measurements (*Bisson et al.*, 2007). In contrast, extracting data from the RPA-derived rasters leaves a raw dataset that measurements can always be checked against, as well as the ability to adjust window sizes for collecting the data as the needs of a study change. However, there were characteristics of the analysis that limited its broad-scale applicability. First, it relied on using wetted variables, in contrast to features like the bankfull width or depth to characterize the geometry of the channel. This was done because some areas with low-lying overhanging vegetation made it impossible to accurately determine the extent of the bankfull width. When considering the needs of salmonids in the summer, the low flow conditions observed in July are what will be of concern and what will determine the connectivity and distribution of certain channel types across the riverscape. However, for more generalizable results, it could be worthwhile to consider variables like the bankfull width, or the bankfull depth, which are less tied to the wetted conditions observed at the time of the survey.

Despite the limitations of the PCA, and classification schemes in general, they remain a valuable tool in aiding the understanding of stream systems. These methods provide a tool to facilitate the rapid, objective and unsupervised classification of channel morphologies at the basin-scale, a scale identified of great importance for the life histories of some aquatic species, but notoriously difficult to characterize. Future studies conducted at this scale, along with observation of aquatic species across multiple watersheds, may lead to greater understanding of the influence that basin-scale patterns in aquatic habitat may have on some aquatic species, thereby helping to fully realize the utility of the Riverscape Approach.

3.5 Conclusion

The methods illustrated in this chapter provide a rapid and objective technique for characterizing patterns in aquatic habitat at the basin-scale of a small, forested channel. This is an environment of historic importance for aquatic species like coho salmon (*Tschaplinski and Pike*, 2017), yet has not benefited from the large scale and high resolution analysis of aquatic habitat facilitated through remote sensing that larger streams have experienced. Use of RPA-derived rasters of bed morphology, bathymetry, and grain size in combination with a PCA-clustering analysis of the channel morphology at 1-metre intervals provided characterization of this channel at an extent that would be difficult to attain using traditional methods. This allowed for the analysis of the channel's local diversity at the basin-scale, and investigation of the necessary scale required to capture its heterogeneity. For Carnation Creek, this was observed to be approximately 200 m. The implications of this research are twofold. First, prior to setting up monitoring experiments, care needs to be taken to ensure that the cumulative sum of the study sections at least equals this scale length. Second, investigation of the local diversity across the channel would help to ensure that study sections are well distributed between areas of high and low diversity. Future research could involve a paired catchment analysis to assess how diversity indexes vary between catchments with different controlling factors (e.g. land-use), to assess if diversity may be a proxy for habitat suitability. Ultimately, these results help to provide a means of bringing novel techniques used in larger systems to the challenging conditions provided by small, forested river systems. This will hopefully help to provide an opportunity for greater riverscape analysis in these systems.

Chapter 4

Conclusion

The methodologies presented in this thesis advance the ability of stream scientists to objectively characterize small, forested mountain channels at the basin-scale using high resolution RPA imagery. Small, forested streams have long been notoriously challenging to characterize using both traditional field and remote sensing techniques, by nature of their dense canopies and challenging topography. Nonetheless, their importance cannot be understated, as seen by the strong preference of salmonids like coho salmon and cutthroat trout for these systems (*Rosenfeld et al.*, 2000). The overall aim of this research was to provide tools to aid in the understanding of these systems through developing a rapid RPA-survey for extracting relevant channel metrics, so as to objectively characterize patterns in channel morphology at the basin-scale. To do this, new techniques were required for the sub-canopy characterization of the system. Chapters 2 and 3 detail these new techniques and test their application to the larger stream network.

The research objective for Chapter 2 was to test the utility of a close range, sub-canopy RPA-survey for characterizing a small, forested mountain channel. The closed canopy and riparian vegetation of the channel precluded the ability to characterize the channel banks using the vertical imagery that has dominated flight plans for stream surveys to date. This challenge was overcome through the inclusion of oblique-convergent imagery that facilitated characterization of hidden portions of the channel banks. An in-depth accuracy assessment was conducted to investigate the difference in vertical error of checkpoints in DEMs created through different flight path configurations. The assessment revealed that the inclusion of oblique imagery provided greater coverage of the channel bed, as well as comparable vertical errors to a flight plan with only vertical imagery. The vertical errors were within the cm scale, which is suited to the reach-scale geomorphic analysis these data would generally be used for. Techniques developed in previous studies were also successfully applied to the imagery for extracting bathymetry and grain sizes across the channel, yielding similar error estimates to those reported in other studies. Application of this new data collection technique can provide geomorphologists with the necessary tools to characterize patterns in channel characteristics such as grain size, water depths and topography across the riverscape.

Building upon the methodology and channel data extracted in Chapter 2, the third chapter provides a means of rapidly and objectively characterizing patterns in channel morphology. Using a PCA and variables grounded in a theoretical understanding of channel form, pool-riffle, transitional and plane-bed morphologies were classified continuously across the stream network. The PCA-clustering technique is less subjective than a traditional observation-based characterization of channel morphology across the stream network, and avoids the potential for the human perception of the channel to influence the classification of channel form. The scale investigated was also greater than what would be easily attainable using traditional methods that yield a similar dataset, such as a total station topographic survey. This is of importance, as the scale investigated with the RPA is a better match to the life cycles completed by some aquatic species in the system (*Fausch et al.*, 2002). Through assessing the patterns in channel diversity across the riverscape, the necessary scale required to capture the stream's heterogeneity was also investigated.

Altogether, this dissertation demonstrates how the capabilities of RPA technology can be used to improve the understanding of small forested mountain channels. The primary contributions to fluvial geomorphology and ecology are:

- A new methodology using sub-canopy and oblique-convergent imagery to characterize the topography, grain size and bathymetry of small, forested mountain channels.
- Demonstration of the applicability of this technique to surveying channels at a resolution and extent relevant to the life cycles of some aquatic species.
- A new framework for the rapid and objective characterization of channel morphology at the basin-scale using easily extractable channel features, and application of these data to investigating patterns in channel diversity across the riverscape.

From a management perspective, these contributions can be applied to streams to provide a holistic view of channel morphology across the riverscape that will allow for the assessment of the links between channel morphology and aquatic species at the riverscape scale. Indeed, given the varying geology, climate and land-use conditions along streams, it is expected that individual streams will display unique characteristics. This leads to the timely research question postulated by *Lapointe* (2012), "How does the unique structure of a riverscape affect salmonid community composition, population size, and stability?". Through incorporation of the techniques illustrated in this chapter, geomorphologists are now in a position to address the physical habitat component of this question. With advances in the ability to study fish at this same scale, the ability to fully realize the utility and potential of the Riverscape Approach is being approached.

Bibliography

Abalharth, M., M. A. Hassan, B. Klinkenberg, V. Leung, and R. McCleary (2015), Using LiDAR to characterize logjams in lowland rivers, *Geomorphology*, *246*, 531–541, doi:10.1016/j.geomorph.2015.06.036.

Agüera-Vega, F., F. Carvajal-Ramírez, and P. Martínez-Carricondo (2016), Accuracy of digital surface models and orthophotos derived from unmanned aerial vehicle photogrammetry, *Journal of Surveying Engineering*, *143*(2), 04016,025, doi:10.1061/(asce)su.1943-5428.0000206.

Anonymous (1996), *Channel assessment procedure: Field guidebook*, 95 pp., Ministry of Forest and British Columbia Environment, Victoria, British Columbia.

Beechie, T. J., D. A. Sear, J. D. Olden, G. R. Pess, J. M. Buffington, H. Moir, P. Roni, and M. M. Pollock (2010), Process-based Principles for Restoring River Ecosystems, *BioScience*, *60*(3), 209–222, doi:10.1525/bio.2010.60.3.7.

Bird, S., D. Hogan, and J. Schwab (2010), Photogrammetric monitoring of small streams under a riparian forest canopy, *Earth Surface Processes and Landforms*, *35*(8), 952–970, doi:10.1002/esp.2001.

Bisson, P. A., K. Sullivan, and J. L. Nielsen (1988), Channel hydraulics, habitat use, and body form of juvenile coho salmon, steelhead, and cutthroat trout in streams, *Transactions of the American Fisheries Society*, *117*(3), 262–273, doi:10.1577/1548-8659(1988)117<0262:CHHUAB>2.3.CO;2.

Bisson, P. A., J. M. Buffington, and D. R. Montgomery (2007), Valley segments, stream reaches, and channel units, *Methods in Stream Ecology*, pp. 23–49, doi:10.1016/B978-012332908-0.50004-8.

Bisson, P. A., J. B. Dunham, and G. H. Reeves (2009), Freshwater ecosystems and resilience of Pacific Salmon: Habitat management based on natural variability, *Ecology and Society*, *14*(1), doi:10.5751/ES-02784-140145.

Borchers, H. W. (2018), *pracma: Practical Numerical Math Functions*, r package version 2.2.2.

Brardinoni, F., and M. A. Hassan (2007), Glacially induced organization of channel-reach morphology in mountain streams, *Journal of Geophysical Research: Earth Surface*, *112*(3), 1–18, doi:10.1029/2006JF000741.

Buffington, J., and R. Woodsmith (2003), Fluvial processes in Puget Sound rivers and the Pacific Northwest, *Restoration of Puget Sound Rivers*, (January 2014), 46 – 78.

Carbonneau, P. E., S. N. Lane, and N. E. Bergeron (2004), Catchment-scale mapping of surface grain size in gravel bed rivers using airborne digital imagery, *Water Resources Research*, *40*(7), 1–11, doi:10.1029/2003WR002759.

Carrillo, G. (2014), *vec2dtransf: 2D cartesian coordinate transformation*, r package version 1.1.

Chartrand, S. M., A. M. Jellinek, M. A. Hassan, and C. Ferrer-Boix (2018), Morphodynamics of a width-variable gravel bed stream: New insights on pool-riffle formation from physical experiments, *Journal of Geophysical Research: Earth Surface*, *123*(11), 2735–2766, doi:10.1029/2017JF004533.

Church, M. (1992), Channel morphology and typology, in *The Rivers Handbook*, edited by P. Carlow and G. Petts, pp. 126–143, Blackwell, Oxford, UK.

Church, M. (2006), Bed material transport and the morphology of alluvial river channels, *Annual Review of Earth and Planetary Sciences*, *34*(1), 325–354, doi:10.1146/annurev.earth.33.092203.122721.

Church M. (2002), Geomorphic thresholds in riverine landscapes, *Freshwater Biology*, *47*, 541–557.

Dietrich, J. T. (2014), Application of structure-from-motion photogrammetry to fluvial geomorphology, *PhD Thesis*, (December), 109.

Dietrich, J. T. (2017), Bathymetric structure-from-motion: extracting shallow stream bathymetry from multi-view stereo photogrammetry, *Earth Surface Processes and Landforms*, *42*(2), 355–364, doi:10.1002/esp.4060.

Fausch, K. D., C. E. Torgersen, C. V. Baxter, and H. W. Li (2002), Landscapes to riverscapes : Bridging the gap between research and conservation of stream fishes, *Bioscience*, *52*(6), 483–498, doi:10.1641/0006-3568(2002)052[0483:LTRBTG]2.0.CO;2.

Flener, C., M. Vaaja, A. Jaakkola, A. Krooks, H. Kaartinen, A. Kukko, E. Kasvi, H. Hyyppä, J. Hyyppä, and P. Alho (2013), Seamless mapping of river channels at high resolution using mobile liDAR and UAV-photography, *Remote Sensing*, *5*(12), 6382–6407, doi:10.3390/rs5126382.

Flitcroft, R. L., K. M. Burnett, G. H. Reeves, and L. M. Ganio (2012), Do network relationships matter? Comparing network and instream habitat variables to explain densities of juvenile coho salmon (Oncorhynchus kisutch) in mid-coastal Oregon, USA, *Aquatic Conservation: Marine and Freshwater Ecosystems*, *22*(3), 288–302, doi:10.1002/aqc.2228.

Flynt, A., and N. Dean (2016), A survey of popular R Packages for cluster analysis , *Journal of Educational and Behavioral Statistics*, *41*(2), 205–225, doi:10.3102/1076998616631743.

Frissell, C. A., W. J. Liss, C. E. Warren, and M. D. Hurley (1986), A hierarchical framework for stream habitat classification: Viewing streams in a watershed context, *Environmental Management*, *10*(2), 199–214, doi:10.1007/BF01867358.

Garcia, X. F., I. Schnauder, and M. T. Pusch (2012), Complex hydromorphology of meanders can support benthic invertebrate diversity in rivers, *Hydrobiologia*, *685*(1), 49–68, doi:10.1007/s10750-011-0905-z.

Harris, C., M. Thoms, and M. Scown (2009), The ecohydrology of stream networks, *International Association of Hydrological Sciences*, *328*, 127–136.

Hartigan, J. A., and M. A. Wong (1979), Algorithm AS 136: A k-means clustering algorithm, *Applied Statistics*, *28*(1), 100, doi:10.2307/2346830.

Hartman, G. F., B. C. Andersen, and J. C. Scrivener (1982), Seaward movement of coho salmon (Oncorhynchus kisutch) fry in Carnation Creek, an unstable coastal stream in British Colombia, *Canadian Journal of Fisheries and Aquatic Sciences*, *39*(4), 588–597, doi:10.1139/f82-083.

Harwin, S., A. Lucieer, and J. Osborn (2015), The impact of the calibration method on the accuracy of point clouds derived using unmanned aerial vehicle multi-view stereopsis, *Remote Sensing*, *7*(9), 11,933–11,953, doi:10.3390/rs70911933.

Hawkins, C. P., J. L. Kershner, P. A. Bisson, M. D. Bryant, L. M. Decker, S. V. Gregory, D. A. McCullough, C. K. Overton, G. H. Reeves, R. J. Steedman, and M. K. Young (1993), A hierarchical approach to classifying stream habitat features, *Fisheries*, *18*(6), 3–12, doi:10.1577/1548-8446(1993)018<0003:AHATCS>2.0.CO;2.

Henry, N. (2018), Geogames and geoplay: game-based approaches to the analysis of geo-information, in *Geogames and geoplay: game-based approaches to the analysis of geo-information*, edited by O. Ahlqvis and C. Schlieder, pp. 177–194, Springer International Publishing, doi:10.1007/978-3-319-22774-0$_9$.

Hugue, F., M. Lapointe, B. C. Eaton, and A. Lepoutre (2016), Satellite-based remote sensing of running water habitats at large riverscape scales : Tools to analyze habitat heterogeneity for river ecosystem management, *Geomorphology*, *253*, 353–369, doi:10.1016/j.geomorph.2015.10.025.

James, M. R., and S. Robson (2014), Mitigating systematic error in topographic models derived from UAV and ground-based image networks, *Earth Surface Processes and Landforms*, *39*(10), 1413–1420, doi:10.1002/esp.3609.

James, M. R., S. Robson, S. D'Oleire-Oltmanns, and U. Niethammer (2017), Optimising UAV topographic surveys processed with structure-from-motion: Ground control quality, quantity and bundle adjustment, *Geomorphology*, *280*, 51–66, doi:10.1016/j.geomorph.2016.11.021.

Jolliffe, I. (2002), *Principal Component Analysis*, Springer Series in Statistics, Springer-Verlag, New York, doi:10.1007/b98835.

Kim, M., and M. Lapointe (2011), Regional variability in Atlantic salmon (Salmo salar) riverscapes: A simple landscape ecology model explaining the large variability in size of salmon runs across Gaspé watersheds, Canada, *Ecology of Freshwater Fish*, *20*(1), 144–156, doi:10.1111/j.1600-0633.2010.00471.x.

Lane, E. (1955), The importance of fluvial geomorphology in river hydraulic engineering, in *Proceedings*, pp. 1–17, American Society of Civil Engineers.

Lapointe, M. (2012), River geomorphology and salmonid habitat: Some examples illustrating their complex association, from redd to riverscape scales, *Gravel-Bed Rivers: Processes, Tools, Environments*, pp. 191–215, doi:10.1002/9781119952497.ch17.

Legleiter, C. J. (2012), Remote measurement of river morphology via fusion of LiDAR topography and spectrally based bathymetry, *Earth Surface Processes and Landforms*, *37*(5), 499–518, doi:10.1002/esp.2262.

Leung, E. S., J. S. Rosenfeld, and J. R. Bernhardt (2009), Habitat effects on invertebrate drift in a small trout stream: Implications for prey availability to drift-feeding fish, *Hydrobiologia*, *623*(1), 113–125, doi:10.1007/s10750-008-9652-1.

Lindenschmidt, K.-E., and J. Long (2013), A GIS approach to define the hydro-geomorphological regime for instream flow requirements using geomorphic response units (GRU), *River Systems*, *20*(3-4), 261–275, doi:10.1127/1868-5749/2012/0053.

Liu, N., A. Harwood, J. Kells, and K.-E. Lindenschmidt (2017), A geospatial model for characterizing the fish resources of the Similkameen River, British Columbia, Canada BYU ScholarsArchive Citation, *Open Water Journal*, *4*(1).

Lloyd, M., and R. . J. . Ghelardi (1964), A Table for Calculating the ‘ Equitability ’ Component of Species Diversity, *Journal of Animal Ecology*, *33*(2), 217–225.

MacVicar, B., H. Piegay, A. Henderson, F. Comiti, C. Oberlin, and E. Pecorari (2009), Quantifying the temporal dynamics of wood in large rivers: field trials of wood surveying, dating, tracking, and monitoring techniques, *Earth Surface Processes and Landforms*, *34*(15), 2031–2046, doi:10.1002/esp.1888.

Mayer, C., and T. P. Kersten (2018), A Comprehensive Workflow to Process UAV Images for the Efficient Production of Accurate Geo-information A Comprehensive Workflow to Process UAV Images for the Efficient Production of Accurate Geo-information, *IX Conferencia Nacional de Cartografia e Geodesia*, (November), 1–8.

McKean, J., D. Nagel, D. Tonina, P. Bailey, C. W. Wright, C. Bohn, and A. Nayegandhi (2009), Remote sensing of channels and riparian zones with a narrow-beam aquatic-terrestrial LIDAR, *Remote Sensing*, *1*(4), 1065–1096, doi:10.3390/rs1041065.

Meissner, A. G. N., M. K. Carr, I. D. Phillips, and K.-e. Lindenschmidt (2016), Using a geospatial model to relate fluvial geomorphology to macroinvertebrate habitat in a geomorphic typologies, (March), 1–17, doi:10.3390/w8020042.

Montgomery, D. R., and J. M. Buffington (1997), Channel-reach morphology in mountain drainage basins, *Bulletin of the Geological Society of America*, *109*(5), 596–611, doi:10.1130/0016-7606(1997)109<0596:CRMIMD>2.3.CO.

Muste, M., D. Kim, and V. Merwade (2012), Modern digital instruments and techniques for hydrodynamic and morphologic characterization of river channels, in *Gravel-Bed Rivers*, pp. 315–341, John Wiley & Sons, Ltd, Chichester, UK, doi:10.1002/9781119952497.ch24.

Naman, S. M., J. S. Rosenfeld, L. C. Third, and J. S. Richardson (2017), Habitat-specific production of aquatic and terrestrial invertebrate drift in small forest streams: implications for drift-feeding fish, *Canadian Journal of Fisheries and Aquatic Sciences*, *74*(8), 1208–1217, doi:10.1139/cjfas-2016-0406.

Naman, S. M., J. S. Rosenfeld, P. M. Kiffney, and J. S. Richardson (2018), The energetic consequences of habitat structure for forest stream salmonids, *Journal of Animal Ecology*, *87*(5), 1383–1394, doi:10.1111/1365-2656.12845.

Nelson, M. C., M. D. Hocking, J. N. Harding, J. M. Harding, and J. D. Reynolds (2015), Quantifying the effects of stream habitat on populations of breeding Pacific salmon, *Canadian Journal of Fisheries and Aquatic Sciences*, *72*(10), 1469–1476, doi:10.1139/cjfas-2014-0253.

Nestler, J. M., C. Baigún, and I. Maddock (2016), Achieving the aquatic ecosystem perspective: integrating interdisciplinary approaches to describe instream ecohydraulic processes, *River Science: Research and Management for the 21st Century*, (i), 84–102.

Notebaert, B., G. Verstraeten, G. Govers, and J. Poesen (2009), Qualitative and quantitative applications of LiDAR imagery in fluvial geomorphology, *Earth Surface Processes and Landforms*, *34*(2), 217–231, doi:10.1002/esp.1705.

Ortega-Terol, D., M. A. Moreno, D. Hernández-López, and P. Rodríguez-Gonzálvez (2014), Survey and classification of large woody debris (LWD) in streams using generated low-cost geomatic products, *Remote Sensing*, *6*(12), 11,770–11,790, doi:10.3390/rs61211770.

Pfeiffer, A. M., and N. J. Finnegan (2017), Basin-scale methods for predicting salmonid spawning habitat via grain size and riffle spacing, tested in a California coastal drainage, *Earth Surface Processes and Landforms*, *42*(6), 941–955, doi:10.1002/esp.4053.

Pojar, J., K. Klinka, and D. A. Demarchi (1991), Coastal western hemlock zone, *Special Report Series 6: Ecosystems of British Columbia*, pp. 95–111.

R Core Team (2018), *R: A Language and Environment for Statistical Computing*, R Foundation for Statistical Computing, Vienna, Austria.

Reid, D. A., M. A. Hassan, S. Bird, and D. Hogan (2019), Spatial and temporal patterns of sediment storage over 45 years in Carnation Creek , BC , a previously glaciated mountain catchment, doi:10.1002/esp.4595.

Rosenfeld, J., M. Porter, and E. Parkinson (2000), Habitat factors affecting the abundance and distribution of juvenile cutthroat trout (Oncorhynchus clarki) and coho salmon (Oncorhynchus kisutch), *Canadian Journal of Fisheries and Aquatic Sciences*, *57*(February), 766–774, doi:10.1139/f00-010.

Rosgen, D. L. (1994), A classification of natural rivers, *Catena*, *22*, 169–199.

Sanz-Ablanedo, E., J. H. Chandler, J. R. Rodríguez-Pérez, and C. Ordóñez (2018), Accuracy of Unmanned Aerial Vehicle (UAV) and SfM photogrammetry survey as a function of the number and location of ground control points used, *Remote Sensing*, *10*(10), doi: 10.3390/rs10101606.

Schlosser, I. J. (1991), Stream fish ecology: A landscape perspective, *BioScience*, *41*(10), 704–712, doi:10.2307/1311765.

Shannon, C. E., and W. Weaver (1964), *The mathematical theory of communication*, 21–33 pp., Urbana: University of Illinois Press.

Tamminga, A. (2016), UAV-based remote sensing of fluvial hydrogeomorphology and aquatic habitat dynamics, (September).

Tamminga, A., C. Hugenholtz, B. Eaton, and M. Lapointe (2015), Hyperspatial remote sensing of channel reach morphology and hydraulic fish habitat using an unmanned aerial vehicle (UAV): A first assessment in the context of river research and management, *River Research and Applications*, *31*(3), 379–391, doi:10.1002/rra.2743.

Tonina, D., and J. M. Buffington (2009), Hyporheic exchange in mountain rivers I : Mechanics and environmental effects, *3*, 1063–1086.

Tonkin, T. N., and N. G. Midgley (2016), Ground-control networks for image based surface reconstruction: An investigation of optimum survey designs using UAV derived imagery and structure-from-motion photogrammetry, *Remote Sensing*, *8*(9), 16–19, doi: 10.3390/rs8090786.

Tschaplinski, P. J., and R. G. Pike (2017), Carnation Creek watershed experiment—long-term responses of coho salmon populations to historic forest practices, *Ecohydrology*, *10*(2), doi: 10.1002/eco.1812.

Wackrow, R., and J. H. Chandler (2011), Minimising systematic error surfaces in digital elevation models using oblique convergent imagery, *Photogrammetric Record*, *26*(133), 16–31, doi:10.1111/j.1477-9730.2011.00623.x.

Wallington, T. J., R. J. Hobbs, and S. A. Moore (2005), Implications of current ecological thinking for biodiversity conservation: A review of the salient issues, *Ecology and Society*, *10*(1), doi:10.5751/ES-01256-100115.

White, S. M., F. J. Rahel, F. J. R. Ahel, S. M. White, and F. J. Rahel (2008), Complementation of habitats for Bonneville cutthroat trout in watersheds influenced by beavers, livestock, and drought, *Transactions of the American Fisheries Society*, *137*(3), 881–894, doi:10.1577/T06-207.1.

Woodget, A. S., and R. Austrums (2017), Subaerial gravel size measurement using topographic data derived from a UAV-SfM approach, *Earth Surface Processes and Landforms*, *42*(9), 1434–1443, doi:10.1002/esp.4139.

Woodget, A. S., R. Austrums, I. P. Maddock, and E. Habit (2017), Drones and digital photogrammetry: from classifications to continuums for monitoring river habitat and hydromorphology, *Wiley Interdisciplinary Reviews: Water*, *4*(4), e1222, doi:10.1002/wat2.1222.

Wyrick, J. R., A. E. Senter, and G. B. Pasternack (2014), Revealing the natural complexity of fluvial morphology through 2D hydrodynamic delineation of river landforms, *Geomorphology*, *210*, 14–22, doi:10.1016/j.geomorph.2013.12.013.

Yilmaz, C. S., V. Yilmaz, and O. Gungor (2017), Ground filtering of a uav-based point cloud with the cloth simulation filtering algorithm.

Zhang, W., J. Qi, P. Wan, H. Wang, D. Xie, X. Wang, and G. Yan (2016), An easy-to-use airborne LiDAR data filtering method based on cloth simulation, *Remote Sensing*, *8*(6), 1–22, doi:10.3390/rs8060501.